Recent progress in the quantitative assessment and interpretation of photoactivity

Uriel Caudillo-Flores, Mario J. Muñoz-Batista, Marcos Fernández-García & Anna Kubacka

Published online: 20 Jun 2022.

Submit your article to this journal ⬀

Article views: 156

View related articles ⬀

View Crossmark data ⬀

Recent progress in the quantitative assessment and interpretation of photoactivity

Uriel Caudillo-Flores[a], Mario J. Muñoz-Batista[b], Marcos Fernández-García[c], and Anna Kubacka[c]

[a]Universidad Nacional Autónoma de México, Centro de Nanociencias y Nanotecnología, Ensenada, Mexico; [b]Department of Chemical Engineering, University of Granada, Granada, Spain; [c]Instituto de Catálisis y Petroleoquímica, CSIC, Madrid, Spain

ABSTRACT

The development of the photo-catalysis field is limited by a deficient quantitative assessment of photo-activity. The interplay between mass and momentum transport together with radiative transfer phenomena taking place at any photo-catalytic reaction or process makes complex such quantitative assessment. To reach this goal, the review studies the measurement, meaning, and analysis of three types of observables. The first family of observables has the reaction rate and closely connected observables as the turnover frequency as central pieces. The second family owns the so-called efficiency observables, starting from the photonic yield and quantum efficiency of the reaction and ending in the global efficiency of the process. Finally, the review studies kinetic constant observables. The contribution focusses on most rencet contribution analyzing these observables in terms of their (adequate) measurement conditions and physico-chemical interpretation, in order to unveil their full potential in the context of the photo-catalysis field.

The field of catalytic reactions driven by light has received enormous attention due to its scientific and technological applications.[1] The photo-catalysis research field displays activity within numerous reactions, such as the elimination of pollutants, microorganism inactivation, energy generation or production of added-value chemicals.[2] In addition, it makes use of a broad range of materials, such as the numerous classes of semiconductors (oxides, sulfides, nitrides, perovskites, carbon-containing materials, polyoxometallates, MOFs, etc.) and metals (for example, plasmonic and non-plasmonic, base or noble).[3,4] Finally, it utilizes a high number of different reactor types or configurations in close correspondence with the variety of the chemical processes to be considered.[1–5] This important and wide range of experimental set-ups and procedures lead to the development of a field with potential universal application.

CONTACT Anna Kubacka ak@icp.csic.es Instituto de Catalisis y Petroleoquimica CSIC, c/Marie Curie 2, 28049 Madrid, Spain.

1. The word of photo-catalysis: basic definitions

In spite of the amplitude of the research field and multiple applications, any photo-catalytic reaction can be divided into several basic steps, common to all of them. The initial step is triggered by absorption of light and subsequent generation of an electron (e⁻) hole (h⁺) pair, called exciton. For main photo-catalysts like titanium oxides, light absorption is controlled by the band gap energy of the semiconductor, that is, the energy difference between the top of the valence band and the bottom of the conduction band. The second step is the exciton dissociation. Electrons and holes must be separated if they are to be involved in subsequent chemical redox steps. The exciton ionization energy (sometimes called binding energy) should be lower than the thermal energy if we wish to have a chance for other than recombination processes. The exciton binding energy is mainly controlled by the dielectric constant of the semiconductor. Once dissociated, the next step is charge carrier diffusion to reach the surface of the photo-active materials and be able to interact with reactant molecules. This process is controlled by the charge carrier diffusion coefficient, related to the charge carrier effective mass and collision time, in turn connected with a significant number of physico-chemical properties of the catalytic solid. The fourth step is the charge transfer to the reactant and the photoredox reaction. This depends also on a significant number of physico-chemical properties connecting the (appropriate) electronic levels of the catalyst and reactant(s) as well as of the interface barrier energy. The last step is fluid mechanics, taking place in the reaction medium.[1–6]

As summarized in Figure 1, from a macroscopic point of view all these steps (except in the last one case) take place with participation of a catalyst defined by its spectral response and inherent catalytic properties, activity, selectivity, as well as stability, the latter implying the existence or not of deactivation and regeneration steps. The first column ("photo-catalyst") of Figure 1 describes graphically this task. The Figure thus highlights the need of a phototocatalyst and the two relevant properties to assess photo-activity correspond to the spectral response and catalytic activity. As discussed in next sections, the first (spectral response) is related to the key property to measure photo-activity, the rate of photon absorption (φ).[7,8] This observable defines the number of Einsteins (moles of photons) absorbed by a material per second and relevant volume or surface unit.[7–9] The second parameter, catalytic activity, can be measured using several parameters and observables but it is typically obtained under steady-state (or pseudo-steady-state) conditions or extrapolated at specific conditions (manly result at time tending to zero).[9] We will discuss all of them in next section.

As happens in heterogeneous catalysis and illustrated in the second column of Figure 1, a complete analysis of the photo-chemical reaction would require to define the active center (and its surface density), the reaction mechanism,
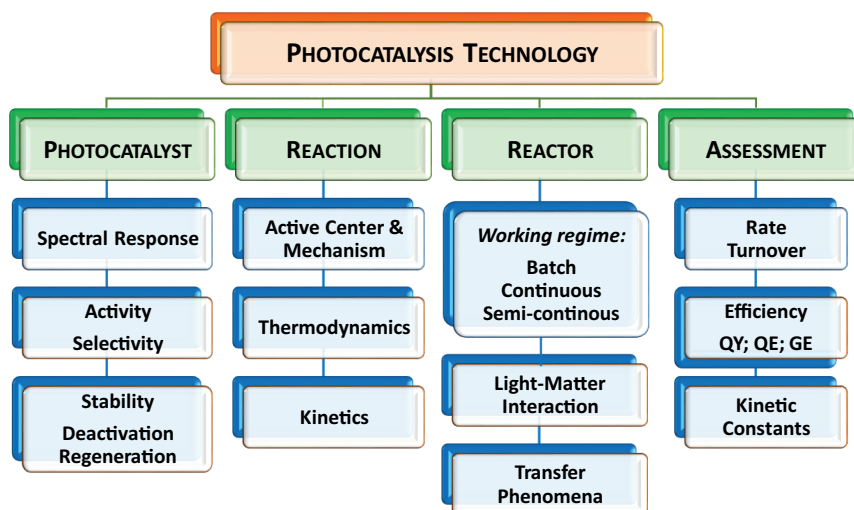
Figure 1. Schematic representation of the photo-catalytic technology. acronyms: QY – quantum yield; QE – quantum efficiency; Ge – global efficiency.

and its thermodynamic and kinetic controlling parameters. We note that the concept of active center is more elusive than the corresponding counterpart in heterogeneous catalysis. This comes from several points but particularly has roots in the fact that any photo-catalytic reaction has initial steps exclusively related with light and not with any of the chemical (reactant) species. What it can certainly have with generality is a rate limiting step whatever it can be and thus, we can associate certain structural/electronic properties of the catalyst controlling this step. Only in the case that the rate limiting step considers the participation of reactant (or intermediates) species we have an unambiguous correspondence with classical heterogeneous catalysis. This point will be discussed in section 2.4. In spite of the complex scenario, column 2 ("reaction") of Figure 1 summarizes this task. In subsequent sections, we present a summary of the current understanding of the mechanisms (including some considerations concerning the active center) as well as thermodynamics and kinetic controlling parameters of photo-catalytic processes (Figure 1). Relatively fruitful efforts have been published toward the analysis of the radical species involved in the key kinetic step and thus the surface radical species connected with the active center. Utilizing mainly optical and electron-paramagnetic resonance tools the involvement of bare holes, $^{\bullet}OH$ (hydroxyl) and $^{\bullet}O_2^{-}$ (superoxide) radicals have been detected in the majority of photo-catalytic mechanisms.[9,10] For example, titanium oxides mostly carry out oxidation reactions using either bare holes or hydroxyl radicals, while carbon nitride utilizes superoxide species and/or bare holes. Besides these reactive species, photo-catalysts generate other radicals with limited kinetic significance, such as hydrogen peroxide (H_2O_2), singlet oxygen ($^1O_2$) and other

radical species. The main point for our purposes is that holes and hydroxyl radicals are present at the surface of most semiconductors in some kind of localized sites. For example, for titanium oxides the presence of Ti-O-Ti-O chains to stabilize bare holes and specific (mono- and bi-dentate) hydroxyl species seems responsible of the formation of the corresponding radical species. Similarly, bare titanium cations and/or anion defects are responsible for the formation of $^\bullet O_2^-$ superoxide radicals.[9,10] Of course, this structural definition of the center where kinetically relevant radical species presumably interact with surface absorbed molecules (whether the reactant or any critical intermediate) is rather limited. It does not give details of the local – medium range environment and other structural/electronic details that strongly affect the number and properties of radical species formed. In addition, and as previously noted, this center could or could not be the active center. In any case, what comes clear from the different studies just outlined is that photo-catalytic mechanisms always involve relatively simple radical species in key controlling steps.

Figure 2 summarizes from a simple point of view the thermodynamics of a photo-catalytic reaction. As described in several sources, due to the essential irreversibility of the charge carrier attack to the target chemical species in photo-catalytic reactions, the necessary and sufficient conditions are that i) the redox potential of a substrate to be reduced (Pred) is lower than the conduction band bottom; and ii) the redox potential of a substrate to be oxidized (Pox) is higher than the valence band top. This set of conditions can allow reactions with apparent (as this does not fully consider the energy input from the photon) positive or negative total Gibbs energy. However, as far as electron and holes chemical reaction channels are irreversible, a negative Gibbs energy (for the global reaction) drives to feasible (photo)-chemical reactions. The mentioned irreversibility is normally a consequence of spatially (taking place
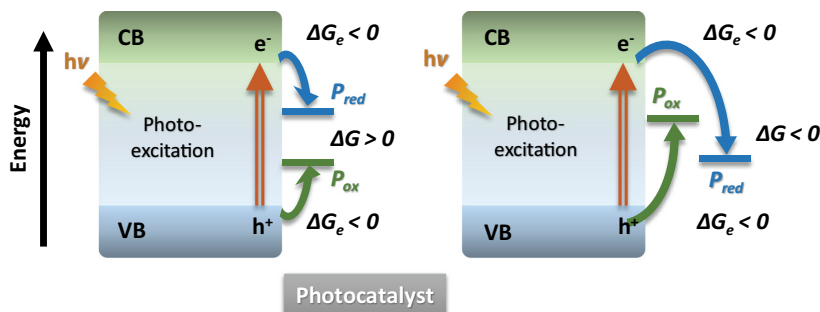

Figure 2. Electronic structure of a semiconductor photo-catalyst and gibbs energy change taking place in a photo-catalytic reaction. Acronyms: CB/VB: conduction/valence band; P_{red}/P_{ox} substrate to be reduced or oxidized; G; Gibbs function. See text for details. adapted with permission from ref. 11. copyright RSC.

in different components of the photo-catalyst) and/or chemically (charge carrier attack generates chemical species not being able to go back in the reaction mechanism) separated reaction paths.[11,12]

Kinetic studies are mainly based in the mentioned main radical-type mechanisms previously outlined. This clearly differs from classical chemical mechanisms. Rigorous introduction of light into the mechanism leads to the so-called intrinsic-type photo-catalytic reaction mechanisms.[9,13,14] A lot of discussions focus along several aspects of such mechanism but, for our purposes, the first goal is how we can define a meaningful mechanistically derived kinetic analysis of the performance of a photo-catalyst.[9–12,15] The numerous attempts to reach this goal will be presented and critically analyzed in following sections. Particular effort will be thus made in terms of the specific mechanistically derived intrinsic kinetics that can render physico-chemical information, in turn providing the grounds for the assessment of photo-activity and, therefore, contributing to the task summarized in column 2 ("reaction") of Figure 1. In addition, intrinsic kinetics is an essential tool for adequate scaling of all photo-catalytic processes.

The photo-catalytic process needs to be carried out in a reactor, being mostly batch, continuous or semi-continuous configurations used in the field. In a photo-catalytic reactor, the two key aspects to consider (aside of the chemical reaction taking place) are related to the light–matter interaction and diffusion effects. The combination of all physico-chemical phenomena taking place in the reactor command the photo-catalytic process. Such a general challenge is presented in column 3 ("reactor") of Figure 1. So, summarizing, a complete knowledge of the above mentioned properties related to the photo-catalyst, the reaction and the reactor defines (from both scientific and technological points of views) all necessary aspects of a photo-catalytic process.

1.1. Scope of the review

To achieve the knowledge summarized in Figure 1, an essential tool is the quantitative assessment of the photo-activity. This issue is not an easy task due to problems mainly originated from a critical point, it is practically impossible to define accurately the active center of any photo-catalytic reaction. As discussed in several sections of this review, this is essentially beyond current technological capabilities. In spite of it, the literature presents a significant number of observables used to report photo-activity. As illustrated in column 4 ("assessment") of Figure 1, most of the contributions report reaction rates to discuss photo-activity. The turnover concept is sometimes used. Most frequently utilized are the (different) efficiency observables. The IUPAC provides "exact" definitions of the so-called photonic yield (some-times called apparent quantum efficiency) and (true) quantum efficiency observables [16] although

the way of calculating them is not unique and many different analytical-numerical approaches are present in the literature. From them, we can consistently carried out the analysis of the global efficiency of the process. A complementary analysis of the photo-activity requires obtaining the kinetic constant of the rate determining step of the mechanism. As mentioned, the use of light as energy input of the reaction is a singularity in heterogeneous catalysis that should be carefully considered to render meaningful and interpretable (kinetic) results.

The main aim of this contribution is to provide a source describing the most important issues for measuring and interpreting activity on quantitative basis rather than providing an exhaustive view of all experimental and calculation procedures present in the literature. Emphasis is thus put on concepts. Experimental-computational tools are nevertheless carefully discussed to highlight their strengths and weaknesses in terms of the realiability of their output(s). In addition, the review focusses on contributions and concepts leading the progress in the last 10 years, that is, those appearing after the main IUPAC recommendadion source for photo-catalysis.[16] Therefore, section 2 discusses modern aspects for the assessment of all observables measuring photo-activity, attempting to provide a guide of their utility and limitations. We analyze the pros and cons of each observable described in Column 4 of Figure 1 to assess photo-activity and how we can obtain scientific and technological relevant information from them. After complection of the analysis, a summary of the most exciting results and future research directions will be presented in section 3.

2. Measurement of Photo-activity

As described in section 1, the measurement of photo-activity is in itself a research field with significant activity. In this section, we will analyze one by one the main observables utilized in such quest (column 4 of Figure 1). As illustrated in Figure 3, [17] we aim to review all observables used to assess photo-activity, starting from the simplest and broadly used to those which normally require intensive experimental and computational approaches. So, initiating the search for the reaction rate, the most common observable(s) reported in the literature, or turnover observables we will analyze the photonic yield, (true) quantum and global efficiency parameters, and end up with a study of the information extracted from kinetic analyses.

However, before carrying out this work, we will make a simple introduction to transfer phenomena on photo-catalytic reactions. Normally, to obtain a meaningful measurement of activity, results free of transfer limitations (diffusion) would need to be considered. Although this is not always possible in photo-catalysis, it is highly desirable, particularly if the activity of the catalyst(s) is assessed using a single experimental condition. This is a frequent case when reporting, for example, reaction rate values.
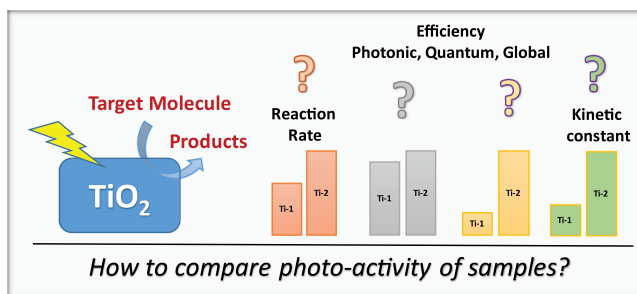
Figure 3. Parameters to assess activity in a series of samples (Ti-1, Ti-2) used in a photo-catalytic reaction. Adapted from ref. 17. Reproduced with permission form Elsevier.

2.1. *A Brief Analysis of Transfer Limitations*

The issue of transfer limitations obviously transcends photo-catalysis. The phenomenon for traditional catalytic processes is widely analyzed in the chemical engineering field and several reactors configurations and specific operation conditions have been developed and well-optimized to reach that goal. Although this issue could be of particular importance for fluidized processes, in reality the contribution of transfer limitation must be carefully controlled to study all (gas and liquid phase) catalytic properties as well as to optimize reactions and carry out rigorous kinetic studies.[18] This section does not attempt to provide a systematic analysis of diffusion but will focus on engineering concepts related to photo-reactors and aiming to rationalize the analysis of the phenomena to quantify properly the photo-catalytic activity.

As it is schematically represented in Figure 4 for a gas phase process, seven elemental steps can be defined. Step 2 describes the diffusion of the molecule from the bulk to the surface of the catalyst. In a typical experiment, the photo-catalyst is a porous nano-particulate solid (e.g. $g-C_3N_4$, TiO_2-based samples), in which both, external and internal catalytic surface (at least part of the solid) are activated by light. The substrates can move from the surface to the internal structure of the material as well. Step 3 is the adsorption of the reactant molecules on the catalytic surface, a phenomenon affected by several chemical and physical properties of the sample such as acidity, pore size, etc. The reaction occurs in light-activated sites, step that is represented as Step 4. The evolution of the products is described by Step 5, followed by Step 6 in which some of the generated products at the internal sites move from the internal porous of the catalyst to its external surface. The final step is the diffusion of the products from the surface to the media. Photochemical interactions of reactants and products summarized by Step 5 concern a relatively complicated process, which demands a deep analysis and is the main subject of this review article. Related to transfer phenomena a key and common issue for all (or the vast majority of) photo-catalytic processes is the non-uniformity of the
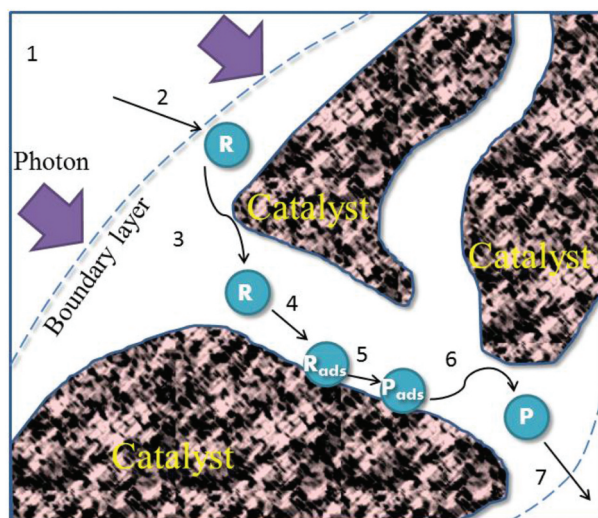
Figure 4. Schematic representation of the mass transfer processes. Reprinted with permission from ref. 19. Copyright Elsevier.

radiation field. In addition, light cannot activate all potential catalytic sites due to void volume or shadowing effects. Both situations are thus inherent to photo-catalysis, meaning that "perfect" homogeneity is not always possible for light-matter-reagents/intermediates interaction processes, producing transfer processes that are difficult to control and understand.[19,20]

2.1.1. Working regimes and rate dependences

Considering conventional thermal catalysis at macroscopic level, if the mass transfer steps are fast, the mass transfer resistance from the bulk to the surface of the catalyst and from the external surface to the internal one in the pore are both negligible. This means that the substrate concentration in the active sites can be considered the same of the bulk concentration, so the mass transfer does not affect the overall reaction rate. If diffusion of the reactants from the bulk to the active sites of catalyst is slow, the external mass transfer resistance is high and becomes a critical issue controlling the overall reaction rate. If the diffusion effects are important and the external mass transfer resistance is negligible, then the substrate concentration profile would vary along the catalyst surface.[21]

A nice and systematic analysis to identify both kinetic and transport regimes during the (liquid-phase) photo-degradation of benzoic acid using titania is illustrated in Figure 5 (panels A and B). A parametric analysis of a slurry set-up was carried out using as main factors the amount of sample, irradiation flux intensity, the initial concentration of benzoic acid and the circulation rate. Using a fixed irradiation flux, Figure 5A describes that the degradation rate was independent of the circulation rate for catalyst
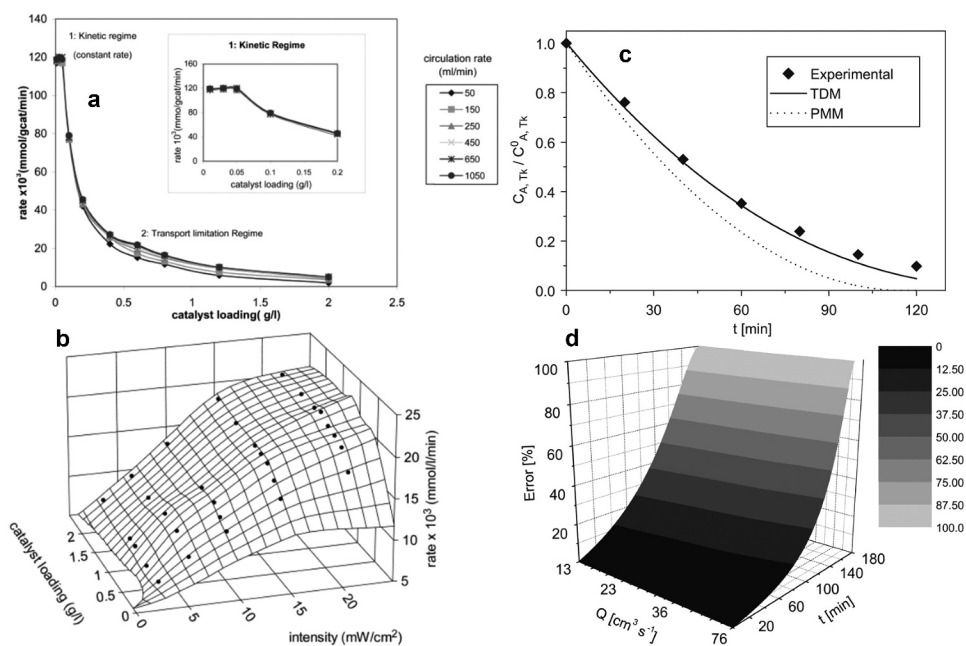
Figure 5. (A) Benzoic acid photodegradation rate at different catalyst loadings and flow rates (light intensity 9.90 mW cm^{-2}). (B) 3D plot of the degradation rate as function of irradiation flux and catalyst concentration. Reprinted with permission from ref. 22. Copyright Elsevier. (C) Experimental data (dichloroacetic acid degradation) and simulation results using TDM (two-dimensional model) and PMM (perfect-mixing model) schemes (flow rate 13 cm^3 s^{-1}; catalyst concentration 2.20×10^{-3} g cm^3). (D) Relative errors between the TDM and PMM models. Reprinted with permission from ref. 23. Copyright Elsevier.

concentration in the 0.01–0.05 g/L region (kinetic regime), while a variable reaction rate was detected when the catalyst amount was increased from 0.05 to 2.0 g/L (transport, mass and/or light, limitation regime). Above 0.05 g/L, the rate decreased gradually with circulation rate, which allows identifying that the overall rate was not fully controlled by kinetics, with a contribution of transport phenomena. For a fixed flow rate, Figure 5B displays the two regimes as a function of two experimental variables; catalyst concentration and irradiation flux intensity. The interaction between experimental parameters will define the regime. As represented in Figure 5B, at any particular irradiation flux intensity, the rate was constant for catalysis concentration greater than ca. 1.25 g/L. However, the rate increased with the increasing of the irradiation flux intensity. In the low region of sample concentration (0.5–1.25 g/L), they describe a "hindered transport" of the molecules to the surface of the sample triggered by the sample agglomeration, while at high loading of the photocatalysts (>1.25 g/L), a "shielding or shadowing effect" takes place. The latter is analyzed by the authors considering that at this condition, the catalyst creates an obstacle for the transport of light to the active surface. This provides a physical interpretation of the specific physico-chemical phenomena defining

the transport limitation regime .[22] The conclusions of authors can be considered of general character. The catalytic conversion can be influenced by several factors, such as (1) the catalyst surface area fraction not in contact with the substrate due to external mass-transfer limitation, (2) the substrate fraction not reaching the catalyst surface area due to agglomeration (internal mass-transfer limitation), (3) light (irradiation flux) limitations to activate all potential catalytic sites by effect of scattering and/or shadowing phenomena.

The phenomenological modeling of reaction systems is an excellent tool for studying the working regime. Comparison of the experimental data and simulation results allows interpreting and quantifying the error made if a wrong model is used in presence of transfer limitations. In Figure 5C, diffusion effects were studied with the help of reactor modeling results obtained using a perfect mixture model (PMM; no diffusion effects) vs. the so-called two-dimensional model (TDM; including diffusion effects). The difference in the output of the models with respect to the experimental data using typical operation conditions (see figure for details) strongly indicates that, as a general rule, mass transfer phenomena must be taken into account. Figure 5D shows the relative errors between the models as a function of the reaction time and the recirculation flow rate for a catalyst amount of 3×10^{-3} g/cm^3. The set of data shows that, using this loading level, the experiment must be performed at high flow rates (or generally speaking strong mixing conditions). The parametric analysis confirmed a strong dependence of the diffusion limitations with the variables; catalyst concentration, irradiation flux, and mixing conditions. Mixing (here facilitated at high flow rates) must always be as efficient as possible, while there is a compensating optimum between the other two parameters. In this particular case, using a concentration of $1x10^{-3}$g/cm^3, the experiment can use the maximum value of the irradiation flux tested (ca. 1.9×10^{-6} Einstein cm^{-3} s^{-1} at the liquid interface facing light source). However, if the concentration of the sample is adjusted, using the same flow condition, the irradiation flux must be reduced proportionally.[23]

2.2. Reaction rate and other closely connected parameters

In (classical, thermal) heterogeneous catalysis a reaction rate measured at differential conditions (e.g. conditions assuring similar reactive atmosphere for the whole catalyst) and/or free of mass transport limitations (perfect mixing) is considered a relatively good and consistent parameter to define the (catalytic) merit of a material.[24] Of course, the analysis of activity requires to study the stability of the catalyst and, focusing in the reaction rate observable, its potential evolution through time. A reaction rate can be expressed by the multiplication of an Arrhenius-type term of the activation energy and temperature and a more or less complex dependence of a term including reactants (and intermediates) concentration(s). Contrastingly to the situation

in heterogeneous catalysis, the reaction rate in heterogeneous photo-catalysis; (i) is usually (although not always as thermo-photo catalytic experiments are also present in the literature) measured at isothermal conditions; and, more importantly, (ii) does show dependence on physico-chemical parameters not mentioned previously in this paragraph.

As it has been demonstrated from the kinetic analyses presented in the literature and summarized in section 2.4 of this contribution, a (correctly measured) photo-catalytic reaction rate always exhibit dependence on the rate of photon absorption (φ) and thus cannot provide chemical information, at least in the straightforward way as it does in the case of heterogeneous catalysis. Light and chemical dependence are both present in the reaction rate and need to be uncoupled to understand the meaning of this parameter. As detailed in the following sections, this can be done using several methods but the most frequently utilized are the analysis of parameters related to the quantum efficiency (to be obtained following the IUPAC rules) as well as parameters coming from intrinsic kinetic models.[16]

In spite of this inherent limitation(s), it is this rather common to compare photo-catalytic reaction rates. Of course, disappearance of the reactant or appearance of the product should be adequately followed and measured. This is not the case in specific reactions like dye degradation, where the bleaching of the product is the parameter scanned in a significant number of measurements reported using optical methods to obtain the corresponding reaction rate(s). Similarly, when studying carbon dioxide reduction several specific analyses like the use of (carbon/hydrogen) isotopic labeling as well as careful checking of production of by-products (like hydrogen and/or oxygen) need to be carried out to provide a real measurement of carbon dioxide consumption. Whether CO_2 reduction or any other complex reaction is considered, a general framework to check the consistency of the reaction rate requires the testing of mass balances. Understanding of the selectivity of the reaction and, generally speaking, considering the balance of carbon in all photo-catalytic reactions but also (for specific reactions) of other elements, such as hydrogen or oxygen of the photo-catalytic reaction (taking into account both the reduction and oxidation counterparts), can provide significant information to ascertain the accuracy/reliability of the rates for reactant disappearance or product generation .[25,26]

In any case, assuming a diffusion-free, robust, and exact measurement of the reactant/product concentration in the outlet stream, several ways of achieving certain level of knowledge about the photo-activity are presented in the literature. Rates of reactant (or product formed) normalized per total mass or catalyst surface area units are frequently utilized.[27,28] The normalization per catalyst mass unit could be more insightful from a technological perspective (highlight the cost of the catalyst in the chemical process) while the surface area normalization may be more informative about the physico-chemical properties (as catalysis takes part at the surface and, in principle, the active site density can

be roughly normalized in this way) affecting activity .[29,30] To make short the discussion, whatever the normalization of the number of reactive species per unit time carried out, none of the resulting observables can render any meaningful information as far as light is not considered explicitly into the calculation.

Yet, for specific kinetics we can extract information from simple methods. For example, if the reaction kinetics follows a Langmuir-type equation where the adsorption constant(s) are independent of light. In such case, we can express the reaction rate as a multiplication of two functions, namely f(Cs) x g(φ); being Cs the concentration of the (relevant) chemical species and φ the rate of photon absorption. The consistency of the separation of variables can be easily checked using spectroscopy. For example, infrared tests to detect vibrational modes of absorbed target molecules, intermediates or products as a function of light intensity and/or contact angle measurements to check hydrophilicity/hydrophobicity changes and potential effects of illumination on water. In any case, only assuming kinetic formalisms allowing separation of variables, analyses based in the behavior of f(Cs) are meaningful. The rationale behind this proposal is summarized in Figure 6 and will be further (and more rigorously) analyzed in section 2.4. As a quantitative descriptor of the f(Cs) behavior, an interesting work proposes to compare different materials using measurements of the corresponding photo-catalyst concentration that allows the reaction rate to reach a plateau.[29] Following such proposal, the plot included in Figure 6 further utilizes a ratio (ξ) between the sample and a reference compound using the "optimum concentration."[31] Of course, as can be immediately deduced from Figure 6, the analysis of the light-dependence of the rate should be also carried out in parallel.
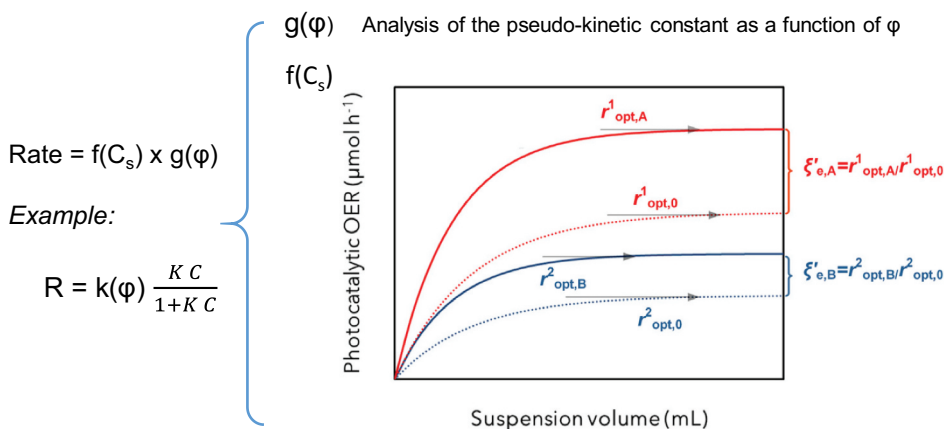

Figure 6. Schematic representation of the analysis of the reaction rate in the case of kinetics allowing separation of chemical and light-related variables. The plot presents the reaction rate measurement (OER; oxygen evolution rate) of two catalysts (A, B) and a reference system (0), as a function of a variable (suspension volume) dependent on catalyst concentration. see text for details. adapted from reference 31. Copyright Elsevier.

A relatively parallel discussion can be carried out for the turnover frequency (TOF) and number (TON) observables. According to the IUPAC, TOF is defined in heterogeneous catalysis as the number of reacting molecules per active site and unit time and is expressed in inverse of time units .[32] The TON results from multiplication of the turnover frequency (TOF) and the lifetime of the catalyst (time). For photo-catalysis, the IUPAC defines TOF as the number of photo-induced transformations (product formed or reactant consumed), per catalytic site and per time period. TON is the number of times, n, that the overall reaction (the photo-chemical transformation) goes through a photo-catalytic cycle.[16] Defining the active site in heterogeneous catalysis is relatively complex but, as mentioned in the previous section, cannot be done (in the vast majority of cases) with current instrumentation and capabilities in heterogeneous photo-catalysis.

Although, we will only discuss the situation briefly, the research aiming to progress in the characterization and understanding of active center(s) of photo-catalytic processes is constantly progressing. On one side, we can highlight the effort carried out and aiming to measure the number of surface sites in titania-related materials. Although a crude simplification of the real reaction active center, it is still a challenging task. In this quest, some interesting approaches utilized titration procedures to analyze the surface Ti sites and for subsequent normalization of reaction rates.[33] Other alternatives (particularly for oxidation reactions) may use •OH (or bare holes) instead of cation (Ti) sites to provide information about surface sites, although their titration using optical, electro-chemical, vibrational, and electron paramagnetic tools cannot render information (mostly cannot isolate from all present species) about the specific hydroxyl (or other) surface species responsible or connected with activity.[9,10,34] As above discussed, as photo-catalytic mechanisms are of radical nature, •OH and the other radical species mentioned in section 1 are relevant in kinetic formalisms and the corresponding limiting step of the reaction rate. On the other side, efforts to interpret rigorously the photo-catalytic reaction from a holistic mechanistic and kinetic view are in continuous progress. This progress is intimately connected with the use of operando and spectro-kinetic schemes.[35,36] New powerful approaches should consider adequate matching between illuminated and probe volumes (otherwise misleading information can be derived) as well as detection capability at molecular level (both for reactant entities as well as catalytic solid surface entities) .[37,38] The latter can be realized with the combined utilization of tools, such as surface enhanced vibrational spectroscopies, modern synchrotron techniques (X-ray absorption and emission, total scattering, etc.), single-particle single-event techniques, and/or time-resolved approaches based in photoluminescence, transient absorption and positron annihilation spectroscopies. The combination of the experimental information with the one coming from theoretical tools (currently based in the use of time-dependent density functional studies of excited states) will complete the picture.[9,35–38]

Summarizing the above discussion, focusing the discussion in the interpretation of the reaction rate, not taking into account light-related features in the assessment of photo-activity leads to limited information that can be only used to compare catalysts at the specific experimental conditions utilized in the experiments.[39] An adequate experimental design (selection of variables) of the photo-catalytic experiments can test a broad range of experimental conditions and can lead (using fitting procedures) to a surface response able to render interesting information about both the light and chemical dependence of the reaction rate.[40,41] In spite of it, the above mentioned parameters (reaction rate, TOF, TON) do not provide *per se* (e.g., directly, without the additional analysis of data) any general (independent of the specific experimental conditions utilized) knowledge about the photo-activity of a material. Nevertheless, the almost standard procedure to partially circumscribe this type of limitation is to include in the measurements a reference material, such as titania P25 Degussa (Evonik), a commercial form of TiO_2 (20 nm nanoparticles, 80% anatase, 20% rutile).[27] This type of approach has been implemented, for example, in two ISO standard procedures for gas-phase NO and acetaldehyde removal reactions.[42,43] These two ISO standard tests also rely on the measurement of the apparent quantum efficiency, an observable discussed below. In other interesting example, the reference sample is used to calculate an excess ratio (or other equivalent observable) to compare a series of catalysts in which each sample rate is reported using the concentration where the rate reaches a plateau.[31] Regardless of the specific method designed in the literature works, the use of a reference material provides a relative benchmark for comparison within a series of different samples as well as with other authors.

In short, the assessment of photo-activity using the reaction rate, TOF and TON observables and based exclusively in catalyst-dependent variables (whatever the case, with or without utilization of reference materials) has inherent limitations, graphically illustrated in Figure 6. A complete framework providing quantitative assessment (i.e., independent of the specific experimental conditions used) of photo-activity using available observables (including the reaction rate) is described in following sections of this review article.

2.3. Efficiency: a central tool for photo-catalysis

As mentioned, the efficiency parameter defines a key family for the measurement and assessment of photo-activity. It can render a quantitative estimation of the any photo-cataytic reaction and process.

2.3.1. Photonic yield and quantum efficiency

According to the IUPAC, calculation of the quantum efficiency requires: (i) measurement of a reaction rate in differential, transfer free conditions (as detailed in section 2.2), typically approached in photo-catalysis by utilizing

initial rates or low conversion conditions measured at optimum experimental conditions including an adequate adsorption (dark) period to ensure equilibrium of the adsorption of reactants; (ii) radiation source reaching steady-state regime; and (iii) incident radiation adequate determined using typically actinometry or radiometry .[16]

From this point and considering a polychromatic source (the common case in photo-catalysis), the apparent quantum yield, correctly termed as photonic yield or efficiency for photo-catalysis, follows the general expression:

$$\eta_p = \frac{\langle r \rangle_A}{\langle q \rangle_A} \times 100 \qquad (3)$$

Where r is the reaction rate expressed in mole per unit volume/surface area and time and q is the net radiation flux reaching the internal surface of the irradiated window, expressed in Einstein per unit time and volume/surface area.

And the quantum efficiency appears as:

$$\eta_q = \frac{\langle r \rangle_A}{\langle e^a \rangle_A} \times 100 \qquad (4)$$

Where e^a is the (local volumetric or surface) rate of photon absorption. Note that all observables are average values (A subindex) calculated over the entire volume/surface of the reaction medium and wavelength range of the illumination source.[16] Due to the inherent non-homogeneity of the photon radiation flux through reactor spatial coordinates, the values of all observables present in equations 3 and 4 are "local" in nature. That is, their values depend on spatial coordinates and have to be adequately averaged.

In both cases, the photonic yield and quantum efficiency, the calculation of the denominator first requires to obtain an accurate measurement of the radiation flux throughout the reaction medium and thus the reactor. As accurate experimental information cannot be obtained due to interference between the probe and light, this unavoidably demands for modeling the light–matter interaction taking place in a photoreactor. Such task utilizes complex experimental and computational procedures and thus "reliable" photonic yield and quantum efficiency values are scarcely present in literature reports. In particular, we can define two main approaches. The first concerns systems where the reaction medium and the catalyst are considered as a single entity to interact with light. These systems are called "pseudo-homogeneous" and a typical example corresponds to suspended catalysts. The second can be called "heterogeneous" and are those where the reaction medium and the catalysts can be separated to analyze their interaction with light. A significant number of systems having supported catalysts can fall into this category. The different approaches to model and solve the light–matter interaction are presented in section 2.3.1.1.

The adequate treatment of the light–matter interaction is nevertheless absent in most cases and values reported in the literature are approximations to real values. This is even a frequent case for reports using the photonic yield. To approximate the calculation of the radiation flux impringing the catalyst, several simplifications are usually considered. Most common are; (i) the consideration of a light source as monochromatic and associating the radiation flux (fluence) of the light source to a central wavenumber; (ii) the utilization of the nominal power of the source or a simple (i.e. not exhaustive testing) evaluation using actinometry/radiometry to obtain the radiation field intensity; and/or (iii) dismissing any physical phenomena other than light absorption in radiation–catalyst interaction.[44,45] The mentioned approximations can lead to significant error in the estimation of the photonic yield. The light sources can have a distribution of flux along a range of wavelengths. Expect in the case of laser sources, minimum of 50 nm are typical. Use of filters may help but to obtain significant intensity it is hard to go below 20 nm. The use of nominal power is essentially misleading for obvious reasons and the measurement using radiometry or actinometry are only real measurements of boundary conditions (as in the vast majority of reactors, the measurement tool will disturb the irradiance and cannot provide a real, spatially resolved, measurement of the radiation flux). Finally, the light–matter interaction needs to consider several physical phenomena besides absorption. As illustrated in Figure 7, in suspended reaction media, scattering of light is as important as absorption while in supported reaction media reflectance is of significance. The contribution of the reactor walls is also neglected in simple approximations. In all cases, the light–matter interaction is reactor, light source and catalyst dependent, and the accuracy of the mentioned estimations/simplifications cannot be predicted with generality. In the most optimistic case, they can render a semi-quantitative radiation flux value. Still many (ISO) standard methods rely in one way or other in these semi quantitate procedures of the photonic yield.[42,43,46]

Another important point comes from the fact that equations 3 and 4 aim to lead to dimensionless parameters, expressed in percentage. In reality, these equations render a magnitude expressed as mole of reactant/product per mole of (incoming or absorbed) photons. The corresponding dimensionless parameters are discussed in section 2.3.2.

2.3.1.1. Light–matter interaction at reaction media. Calculation of equations 3 and 4 requires as main task to make a quantitative analysis of the light–matter interaction governing the physical phenomena taking place in a photocatalytic process. As mentioned, this section presents the main approaches followed in suspended and supported catalysts.
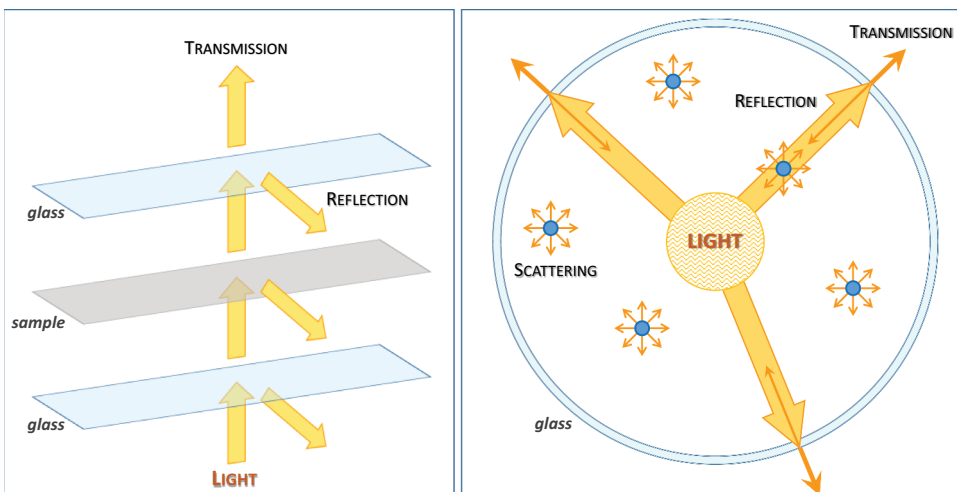
Figure 7. Schematic illustration of main optical events taking place in supported (right) and suspended (left) photo-catalytic processes.

2.3.1.1.1. Obtaining the rate of photon absorption for suspended catalysts. For pseudo-homogeneous systems, the light–matter interaction can be mathematically described by the radiative transfer equation (RTE). It measures the variation of intensity through a direction of the space (s) and associated to a beam of rays of wavelength λ in the direction of a solid angle vector, $\underline{\Omega}$.

$$\frac{dI_{\lambda,\underline{\Omega}}(\underline{x})}{ds} = -\kappa_\lambda(\underline{x})I_{\lambda,\underline{\Omega}}(\underline{x}) - \sigma_\lambda(\underline{x})I_{\lambda,\underline{\Omega}}(\underline{x}) + \frac{\sigma_\lambda(\underline{x})}{4\pi} \int_{\Omega'=4\pi} p\left(\underline{\Omega}' \to \underline{\Omega}\right) I_{\lambda,\underline{\Omega}'} d\underline{\Omega}$$

(5)

Note that $I_{\lambda,\underline{\Omega}}(\underline{x})$ has wavelength, directional, and spatial dependences. In this equation, $\underline{x}$ defines the spatial coordinates of any point of the reactor ("local" value), $\kappa_\lambda(\underline{x})$ is the absorption coefficient; $\sigma_\lambda(\underline{x})$ is the scattering coefficient; and $p\left(\underline{\Omega}' \to \underline{\Omega}\right)$ is the scattering phase, usually measured with the Henyey and Greenstein phase function for photo-catalytic samples.[47] The latter function is expressed as:

$$p\left(\underline{\Omega}' \to \underline{\Omega}\right) = \frac{1 - g_\lambda^2}{\left(1 + g_\lambda^2 - 2g_\lambda u_0\right)^{3/2}}$$

(6)

where g_λ is the so-called asymmetry factor and u_0 is the director cosine between incoming and outgoing light at each point of the space. The g factor takes values between −1 and 1. Negative values indicates that backward scattering dominates, zero corresponds to isotropic scattering, and positive values shows a dominant forward scattering phenomenon. The accuracy of the Henyey and Greenstein phase function has been recently confirmed.[48]

Equation 5 assumes that: (i) the emission radiation is negligible (at fixed temperature near the ambient one), and (ii) steady state condition during the photo-catalytic processes. For non-isothermal process and, particularly, for thermo-photo catalytic processes at temperatures significantly higher than room temperature, assumption (i) is not valid and approximate methods to include the emission term have been presented for suspension (and supported) systems.[49,50] The incident radiation flux at the reactor wall should be taking into account as a boundary condition.

The integro-differential RTE equation is solved by two types of methods, called simplified and rigorous ones. Simplified methods attempt to obtain an economical solution in terms of computational effort and propose a simplified treatment of scattering. They frequently provides analytical expressions to calculate the integral part of equation 5. On the contrary, rigorous methods rely in the numerical solution of the equation and are exact as far as enough computational effort is carried out to obtain a stable (converged value within expected error) solution when increasing the number of numerical steps/ cycles of the spectral/spatial/directional discretization used to solve the integral and differential parts of equation 5 .[51]

In any case, irrespective of the method, the solving of the RTE requires measuring (or obtain from previous information) the optical properties of the system. A dimensional analysis by the Buckingham π theorem of equation 5 indicates that optical dimensionless parameters are the optical thickness ($\beta_\lambda L_0$; where beta is the extinction coefficient, $\beta_\lambda = \kappa_\lambda + \sigma_\lambda$) and the scattering albedo ($\frac{\sigma_\lambda}{\beta_\lambda}$). Thus, the three optical parameters (beta, alpha, and kappa) should be obtained using independent optical measurements. Moreover, the asymmetry factor utilized in the Henyey and Greenstein phase function should be also obtained in the procedure.

The general methodology followed to obtain the mentioned parameters is illustrated in Figure 8. Using a UV spectrometer and a spectroscopic-grade cuvette, the extinction coefficient as well as the reflectance and transmittance of the medium can be measured for the liquid phase (water, water: methanol, or any other reactive mixture utilized in the experiments measuring reaction rates) at different catalyst concentrations. Normally, the cuvette has a rather low light path (0.1–0.5 mm) and the ray propagation through the media can be modeled as a one-dimensional (x parameter in the middle panel of the Figure) one-directional (a single angle along the x coordinate, in the Figure called θ and its cosine μ) phenomenon. The corresponding RTE of the cuvette can be thus solved very fast, considering the cuvette walls (which transmittance and reflectance are experimentally measured) as boundary conditions. The optical coefficients (described at the right of Figure 8) are obtained by a non-linear fitting procedure, which use the transmittance and reflectance as objective functions. This procedure is carried out for a sufficient number of wavelengths
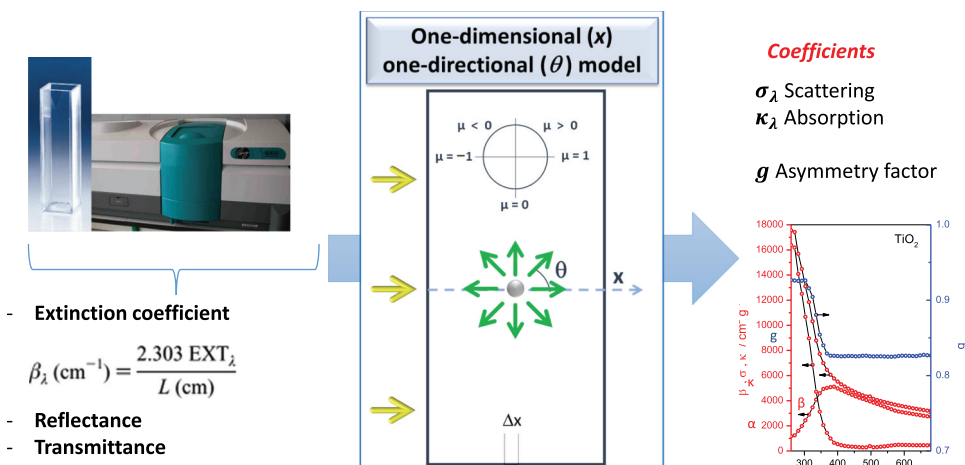
Figure 8. Schematic representation of the procedure to obtain optical-related coefficients for suspended catalysts. Symbols: L length of the cell, x spatial coordinate, θ directional coordinate, and μ director cosine.

to measure the above mentioned coefficients within the emission range of the light source, rendering the result presented at the right for an anatase TiO_2 sample (bottom-right part of Figure 8).[47] The example shows a significant variation of the parameters as a function of the wavelength that needs to be considered in the calculations. Even for relatively limited wavelength ranges of light excitation, this appears as a critical point in order to obtain accurate information to solve posteriorly the RTE in a reactor.[52] Interestingly, we note that recent approaches provide new procedures (yet to be fully tested) to measure the optical properties of the solid suspension using laboratory reactors instead of spectroscopic cells/cuvettes.[53]

Of course, the values of the optical coefficients are specific for the reaction medium but critically depend (particularly the scattering and absorption coefficients) on the primary/secondary particle size of the materials (in turn depending on the catalyst nature and concentration and reaction medium). The size of the aggregates formed in the liquid phase may trigger that certain fraction (internal fraction) of the material cannot be excited by light.[23,54,55] So, this type of "void" volume (closely related terms used in the literature and describing the phenomenon are "shadowing effect," "blocking effect," "shielding effect," "dead volume," etc.) would need to be considered in calculations.

The mathematical-numerical grounds for simplified and rigorous numerical methods to solve the RTE were summarized in classic books.[56,57] As mentioned, they differ in the exact way scattering is modeled in the system. This contribution does not aim to provide a detail review of the works discussing these methods. Yet, we again stress that most utilized "simplified" ones are based in a very coarse directional discretization, such as two-flux models for zero [58] and greater than zero [59,60] reflectance, the six-flux model, [61–63] or others such

the probabilistic approach for dense particulates.[64] As mentioned, they afford economy in calculation at the expense of accuracy.[65,66] Rigorous methods currently utilized are the discrete ordinate method, [67,68] the finite volume method [69,70] and those based in the Mote Carlo type algorithm.[71,72] The latter finds also application as a simplified method and/or to contrast with the output of other methodologies here mentioned. The discrete ordinate method discretizes the RTE and transforms the integro-differential equation in a system of algebraic equations.[73–75] The finite volume method divides the computational domain into a number of control volumes and the solid angle is discretized into a number of finite elements.[76,77] Monte Carlo is not based in the discretization of directional/spatial variables but in the use of random numbers to generate trajectories and fates of the photons existing the light source or entering into the reactor window.[70,78,79] Monte Carlo methods were also used to test experimental set-up(s) to approximately calculate the local volumetric rate of photon absorption using optical measurements at the wall of the reactor.[80,81]

Figure 9 illustrates the main steps to obtain the local volumetric rate of photon absorption. Using the information extracted from Figure 8 and presented at the left of the figure, the task requires, as a central piece, to model the reactor. In the example selected, the incident radiation is apical and needs to be measured using actinometry and/or radiometry. This and the walls of the reactor constitute the boundary conditions. At the corresponding interfaces, transmittance, reflectance, and refraction (the latter particularly at reactor walls) need to be considered.[8,9,47,82] The reactor (central panel) is here analyzed by the discrete ordinate method with a two-dimensional (radius and height, called r and z, respectively) two-directional (two angles, θ and ϕ) model. In this case, the spatial discretization (Δr, Δz) is graphically described in the top plot of the central panel. In the central plot of the central panel, the discretization of the directional variables (represented by their director cosines values, called μ and η) is presented. The procedure selects the director cosines in such a way that it attempts to optimize the integration in equation 5 using Gauss-Legendre quadrature. The bottom figure of the central panel indicates how the boundary conditions have to be coupled to carry out the calculation though the reactor space (this organizes the angular variables in four quadrants that drive the way to link the angular variables variation when the calculation is progressing through space). Whatever the specific method used, the result of the calculation is $I_{\lambda,\underline{\Omega}}(\underline{x})$.[75] After calculation of the intensity, the local volumetric rate of photon absorption ($e^{a,v}$) was computed at each $r - z$ point of the reactor following equation 7.

$$e^{a,v} = \int_\lambda \kappa_\lambda(\underline{x}) \cdot \ _{\Omega=4\pi} I_{\lambda,\underline{\Omega}}(\underline{x}) d\Omega \, d\lambda \tag{7}$$
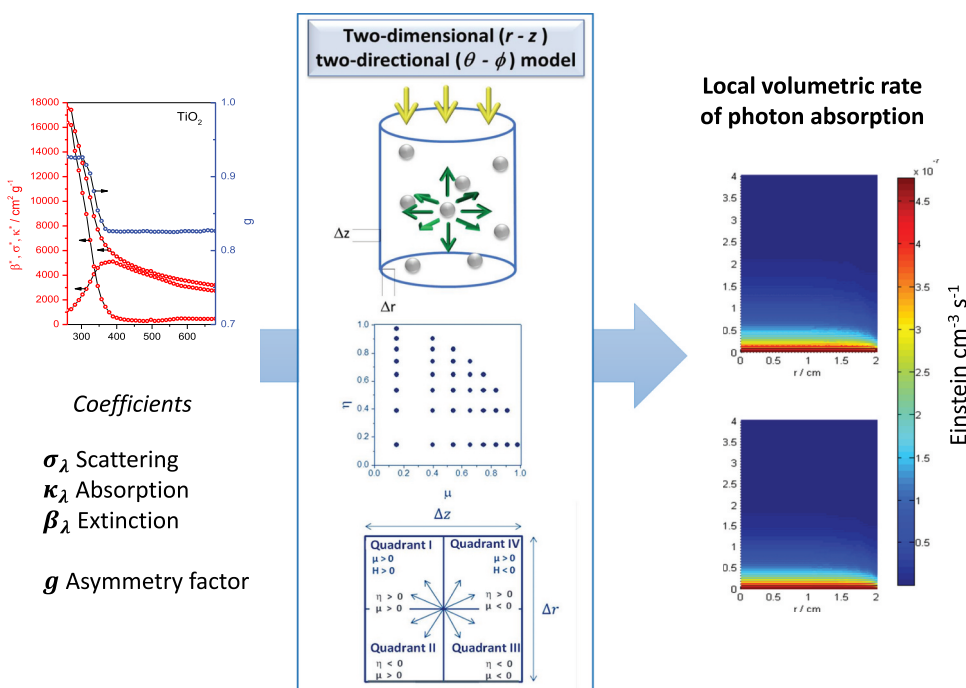
Figure 9. Schematic representation of the procedure to obtain the volumetric rate of photon absorption. Symbols: r,z spatial coordinates, θ,φ directional coordinates, η,μ director cosines.

The integration of the intensity itself is the radiation flux. The panels at the right of Figure 9 show the $e^{a,v}$ observable for a section (r-z) of the reactor. The reactor volume is generated using r-z sections around the polar angle (rotating through the central axis of the reactor, see central panel of Figure 9). By symmetry, they are the same as the one presented. The figure includes two panels corresponding to two different concentrations of the catalyst.

In a brief summary, this section attempts to highlight the standard procedures and main problems to obtain the real ("quantitative") value for the observables described in equations 3 and 4. Both numerical and experimental sources of error should be considered. Considering the denominator of the equations, numerical errors can be avoided with rigorous methods as far as convergence is achieved in the observable values when decreasing the step in the discretization of all variables (spatial, directional, and spectral). This is time consuming but the limit of this process is fixed by the total error expected in the photonic yield or quantum efficiency. The experimental issue can have multiple sources. As discussed above, adequate measurements (and checking) of the optical properties and the radiation flux at boundary conditions is required in order to render meaningful results. As a rule of thumb, typical error in the estimation of the reaction rate is between 5% and 10% and in the volumetric rate of photon absorption can be more than twice. More importantly, the existence of a void volume is, as mentioned, experiment (sample,

light, and reaction medium) dependent and unavoidable in most experimental conditions. Although recognized, the solving of this problem has been, however, dismissed in the literature and requires careful analysis to provide correct values for the observables.[23,26]

2.3.1.1.2. Obtaining the rate of photon absorption for supported catalysts. For a significant number of supported systems, the reaction medium does not participate in the light–matter interaction. When it does, for example, for acetone or dyes in significant concentration and under specific excitation wavelenghts, it can be modeled separately to a good degree of approximation. Also, phenomena taking place at the catalyst and considering (light-absorbing) adsorbed molecules would need to be considered. In any case, when the reaction medium does not participate, the net radiation flux at the internal window of the reactor is the one impinging the catalyst surface, $q_{sup,\lambda}(\underline{x})$.[7] This is the observable to be used to calculate the photonic yield according to the IUPAC.[16] Most of the photo-catalytic processes where supported catalysts are used fall in this "heterogeneous" category. The supported catalyst is utilized and modeled as a thin film.

There are several methods to calculate the $q_{sup,\lambda}(\underline{x})$ observable, all requiring several steps. As outlined in section 1 of this work, we will not review them but just provide a freamework of the main steps and challenges they solve. First, all methods require to model the lamp emission using line, surface, or volume-type emission models.[9,14,83–85] For LED sources cone-shaped or power-cosine models are used.[86] In the central panel of Figure 10 (top plot) the surface emission model is shown as example. The results are typically validated by analyzed the flux vs. distance using radiometry in "empty" space. As said, the direct measurement of radiation flux could be used, however the difficulty of accessing catalyst (and other elements) positions in reactors makes this a more complex option, although some approximations can be carried out in specific cases (or reactor geometries) using optical fibers and adequately designed step-ups to obtain the macroscopic radiant energy balance.[87]

Connecting the lamp emission spectrum ($I_\lambda(\underline{x}, \underline{\Omega})$) with the $q_{sup,\lambda}(\underline{x})$ observable requires more or less complex procedures with several steps. In the middle of the central panel of Figure 10 a model of a cylindrical (co-axial) reactor is shown to illustrate the issue. Glass (in blue) and catalysts (in orange) transmittance and reflectance (experimental measured data at the right part of the figure) would need to be considered to obtain $q_{sup,\lambda}(\underline{x})$. Diffuse and/or specular reflection models are used to account for the reflectance contribution in an energy balance. Refraction mostly for glass/quartz elements (glass/quartz interface with reaction medium) should also be considered.[82,85,88] As schematically presented in the equations included at the bottom of the central panel of Figure 10,
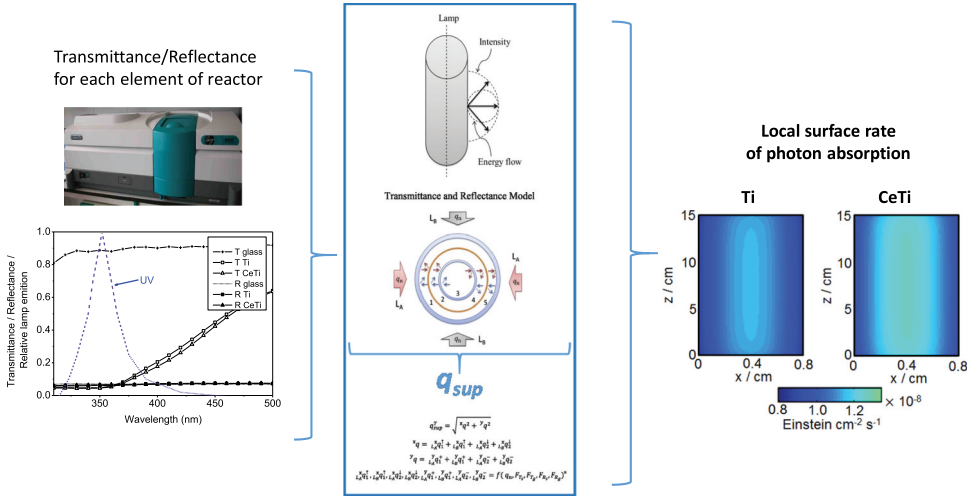
Figure 10. Schematic representation of the procedure to obtain the local superficial rate of photon absorption. Symbols: $^{x,y}q$, x,y spatial components of flux vector q; F_{j_k} Fraction of transmission/reflectance (j = T/R) of the catalyst/glass (k = s/g); Ti, titania sample; CeTi, ceria-titania sample.

the ending result expressed $q_{sup,\lambda}(\underline{x})$ as a complex (geometry dependent) formulae of the transmittance/reflectance/refraction of each reactor element and a flux term $q_{n,\lambda}(x)$. The latter is calculated as:

$$q_{n,\lambda}(x) = \underline{n}_G \underline{q}_\lambda = \int_\Omega I_\lambda(\underline{x}, \underline{\Omega}) \underline{\Omega} \bullet \underline{n}_G \, d\Omega \qquad (8)$$

Where $\underline{n}_G$ is the outwardly directed unit vector normal to the catalytic surface.

Taking into account that the catalyst is a film, the rate of photon absorption is defined per surface unit. So, the local superficial rate of photon absorption (Einstein per surface area and time unit) is defined by:

$$e^{a,s}(\underline{x}) = q_{sup}(\underline{x})F_{As} \qquad (9)$$

Where F_{As} is the fraction of light absorbed by the catalyst (sample). If absorption, reflectance and refraction events describe light–matter interaction, F_{As} can be obtained using classical (geometrical) optics. Note that, through parameters explicitly declared in equation 8, equation 9 requires the integration in lambda over the light source emission spectrum. As example, the value of the $e^{a,s}$ parameter as a function of the surface position of a cylinder (defined by two spatial coordinates) is shown in the panels at the left of Figure 10 for two different (titania and ceria-titania) catalysts. In the example, relatively limited differences in the transmittance and reflectance of the samples (right of Figure 10) lead to a clear difference in the local superficial rate of photon absorption.[89] Finally, if dispersion also takes part in the light–matter interaction (liquid reaction medium in specific cases or catalysts with fractal aggregates specifically designed), a "pseudo-homeneous"

methodology is used to evaluate the photon distribution inside a fixed-bed reactor. These methods used the RTE presented in equation 5 [90] or the Helmotz equation .[91]

To briefly summarize this section, the calculation of the denominator of equations 3 and 4 involves the measurement/modeling of the light source emission as well as all optical phenomena taking place in the reactor elements (including the catalyst). Light source emission is , normally, accurately modeled with the help of an experimental checking of the intensity through distance from the source. For classical "heterogenous" supported catalysts, the light–matter interaction within the reactor can be calculated numerically as equation 9, implying an algebraic relationship with the optical properties of the reactor-catalyst elements [89,92,93] or using Monte Carlo methods.[94–96] Simple models only take into account transmittance (absorbance) events for each element of the reactor. Dismissing the refraction and reflectance can lead, however, to important errors. The accuracy of models presenting a limited representation of the light–matter interaction has been scrutinized in the literature. Dismissing refraction in systems considering air-glass/quartz-air is significantly less problematic than in air-glass/quartz-water.[85] In any case, neglecting reflectance and refraction effects can be from ca. 5 to up to 25–30% error in the local surface rate of photon absorption value, depending on the reaction medium (gas, liquid) and reactor geometry.[85,88,89] If scattering is important in the description of light–matter interaction, the sources of errors were described in the previous subsection. Importantly, in a parallel situation to suspended catalysts, the problem of the void volume, that is, the fraction of catalyst volume not available to the light, is also of importance and often dismissed to obtain photonic yield and quantum efficiency values. As a general result, this problem is a catalyst morphology dependent effect (and therefore specific of the system analyzed). Relevant catalyst morphology properties corresponds to the secondary particle size and porosity properties.[89,97]

2.3.1.2. *Notes on the dimensionality of the efficiency parameters: the chemical problem.* The units of the photonic yield and quantum efficiency parameters (equations 3 and 4) are mole of reactant/product per Einstein (mole of incoming or absorbed photons). This has inherent limitations now discussed.

In this context, introducing "chemical information" into the formulation of the photonic yield and quantum efficiency observables would provide information about the number of charge carrier species utilized in chemical steps per mole of photons. In other words, for the vast majority of cases (excluding charge multiplication or similar phenomena which, in any case, can be easily accounted for in the calculation using a simple constant), it would allow to calculate the fraction of photons generating chemistry from the total incident or absorbed photons.[26] Thus, the corresponding definition of efficiency observables including chemical information drives to dimensionless

parameters and renders a real estimation of the light to chemical energy conversion. Important to note is the fact that such definition is commonly (although unadvertendly) utilized in the literature. For example, when multiplying by two hydrogen photo-production photonic yield or quantum efficiency values, see below.

The mentioned fraction of photons involved in chemical steps can be calculated multiplying denominators of equations 3 and 4 by the factor S defined in equation 10.

$$S = \sum_i n_i S_i \qquad (10)$$

where S is a dimensionless constant connected with the selectivity of the chemical transformation of the molecule considered in the reaction rate. In equation 10, i runs over all products of the reaction, S_i is the fractional selectivity to product i, and n_i is the inverse of number of charge carrier species required to obtain 1 mole of the molecule utilized to express the reaction rate. This factor can be calculated using the number of charge carriers required to produce a single target molecule.[89,98]

To calculate the n_i we can use specific information about the mechanism of the reaction but we only need the overall chemical reaction for each product. If the product(s) is (are) generated in absence of charged species in the reaction medium (typically "free" H^+ or OH^- species are present in water medium with concentrations defined by the pH of solution, but absent at all gas-phase reactions as a consequence of the electroneutrality), we can obtain the values of the n_i observables using charge and atom (the number of independent equations are enough to render a single solution for all photo-catalytic processes) balances. This method can be extended for simple cases where the charge balance cannot be easily predicted but is stoichiometrically simple.

Table 1 compiles, as representative examples, the balanced equations and n_i values for gas-phase oxidation of 2-propanol, [17] toluene, and styrene [99,100] as well as the generation of hydrogen from methanol and ethanol [101,102] and the reduction of carbon dioxide to common products.[103] Liquid-phase 4-Chlorophenol degradation has also been considered.[104] These works utilized titania and carbon nitride-based materials. Table 1 thus considers gas-phase (six examples) and liquid (last entry) phase reactions. As a curiosity, we note that, as far as hydrogen production from methanol (and ethanol) renders the products present in Table 1, no matter the selectivity achieved by the catalyst, the calculation of the S factor multiplies by two the reaction rate, as normally assumed in the literature. Of course, if other product(s) is/are obtained this may not be true. However, most works only reported the products included in Table 1 .[105] Note also, that the reaction rate expressed as methanol/ethanol consumption does not follow such "simple" behavior. On

Table 1. Balanced equations and n values for several photo-catalytic reactions.

2-propanol oxidation; ref. 17

Acetone: $C_3H_8O + \frac{1}{2}O_2 + \frac{1}{2}h^+ + \frac{1}{2}e^- \rightarrow C_3H_6O$ — $n = 2$

Formaldehyde: $C_3H_8O + \frac{7}{2}O_2 + \frac{7}{2}h^+ + \frac{7}{2}e^- \rightarrow CH_2O + 2CO_2 + 3H_2O$ — $n = 2/7$

Carbon dioxide: $C_3H_8O + \frac{9}{2}O_2 + \frac{9}{2}h^+ + \frac{9}{2}e^- \rightarrow 3CO_2 + 4H_2O$ — $n = 2/9$

Styrene oxidation; ref. 99

Styrene Oxide: $C_8H_8 + \frac{1}{2}O_2 + \frac{1}{2}h^+ + \frac{1}{2}e^- \rightarrow C_8H_8O$ — $n = 2$

Benzaldehyde: $C_8H_8 + 2O_2 + 2h^+ + 2e^- \rightarrow C_7H_6O + CO_2 + H_2O$ — $n = 1/2$

Carbon dioxide: $C_8H_8 + 10O_2 + 10h^+ + 10e^- \rightarrow 8CO_2 + 4H_2O$ — $n = 1/10$

Toluene oxidation; ref. 99,100

Benzaldehyde: $C_7H_8 + O_2 + h^+ + e^- \rightarrow C_7H_6O + H_2O$ — $n = 1$

Carbon dioxide: $C_7H_8 + 9O_2 + 9h^+ + 9e^- \rightarrow 7CO_2 + 4H_2O$ — $n = 1/9$

H$_2$ production from methanol; ref. 101

Formaldehyde: $CH_3OH + 2h^+ + 2e^- \rightarrow CHOH + H_2$ — $n = 1/2$

Acetic acid: $CH_3OH + H_2O + 4h^+ + 4e^- \rightarrow CHOOH + 2H_2$ — $n = 1/2$

Methyl formate: $2CH_3OH + 4h^+ + 4e^- \rightarrow C_2H_2O_2 + 2H_2$ — $n = 1/2$

Carbon dioxide: $CH_3OH + H_2O + 6h^+ + 6e^- \rightarrow CO_2 + 3H_2$ — $n = 1/2$

H$_2$ production from ethanol; ref. 101

Acetaldehyde: $C_2H_5OH + 2h^+ + 2e^- \rightarrow C_2H_4OH + H_2$ — $n = 1/2$

Acetic Acid: $C_2H_5OH + H_2O + 4h^+ + 4e^- \rightarrow C_2H_3OOH + 2H_2$ — $n = 1/2$

Ethyl acetate: $2C_2H_5OH + 4h^+ + 4e^- \rightarrow C_4H_7OOH + 2H_2$ — $n = 1/2$

Carbon dioxide: $C_2H_5OH + 3H_2O + 12h^+ + 12e^- \rightarrow 2CO_2 + 6H_2$ — $n = 1/2$

CO$_2$ reduction with water; ref. 103

Carbon oxide: $CO_2 + 2h^+ + 2e^- \rightarrow CO + \frac{1}{2}O_2$ — $n = 1/2$

Formic acid: $CO_2 + H_2O + 2h^+ + 2e^- \rightarrow CHOOH + \frac{1}{2}O_2$ — $n = 1/2$

Formaldehyde: $CO_2 + H_2O + 4h^+ + 4e^- \rightarrow HCHO + O_2$ — $n = 1/4$

Methanol: $CO_2 + 2H_2O + 6h^+ + 6e^- \rightarrow CH_3OH + \frac{3}{2}O_2$ — $n = 1/6$

Methane: $CO_2 + 2H_2O + 8h^+ + 8e^- \rightarrow CH_4 + 2O_2$ — $n = 1/8$

4-Chlorophenol degradation in water; ref. 104

4-chlorocatechol; 4-chlororesorcinol: $C_6H_5ClO + \frac{1}{2}O_2 + \frac{1}{2}h^+ + \frac{1}{2}e^- \rightarrow C_6H_5ClO_2$ — $n = 2$

Hydroquinone, resorcinol: $C_6H_5ClO + 5H_2O + 6h^+ - 2e^- \rightarrow C_6H_6O_2 + 2O_2 + 8H^+ + HCl$ — $n = 1/6$

Benzoquinone: $C_6H_5ClO + \frac{1}{2}O_2 + \frac{1}{2}h^+ + \frac{1}{2}e^- \rightarrow C_6H_4O_2 + HCl$ — $n = 2$

Succinic acid: $C_6H_5ClO + 3H_2O + 2O_2 + 6h^+ + 2e^- \rightarrow C_4H_4O_4 + 2CO_2 + 4H^+ + HCl$ — $n = 1/6$

Maleic acid: $C_6H_5ClO + \frac{26}{4}H_2O + \frac{3}{4}O_2 + \frac{47}{4}h^+ + \frac{3}{4}e^- \rightarrow C_4H_6O_5 + 2CO_2 + 11H^+ + HCl$ — $n = 4/47$

Acrylic acid: $C_6H_5ClO + \frac{14}{4}O_2 + \frac{14}{4}h^+ + \frac{14}{4}e^- \rightarrow C_3H_4O_2 + 3CO_2 + HCl$ — $n = 4/14$

Adipic acid: $C_6H_5ClO + 3H_2O \rightarrow C_6H_{10}O_4 + HCl$ — $n = 0$

Carbon dioxide: $C_6H_5ClO + \frac{13}{2}O_2 + \frac{13}{2}h^+ + \frac{13}{2}e^- \rightarrow 6CO_2 + 2H_2O + HCl$ — $n = 2/13$

the other hand, inspection of the table allows concluding that this singular situation does not take place for the rest of reactions presented. In the case of CO_2 reduction, it can be noted that by-products can depend strongly on the gas or liquid-phase nature of the reaction as well as the specific experimental conditions. Obviously, hydrogen can be always generated as a side reaction from protons and consuming electrons.

The same objective of including chemical information in the photonic yield or quantum efficiency can be always achieved in aqueous liquid phase, that is, in presence of charged species (at least protons/hydroxyls, and typically, inorganic cations/anions containing N, Cl, etc.). However, in this case the balance of charged species requires to measure the pH in order to allow the calculation of the values of the n_i parameters. A basic formulation would indicate that the concentration of protons/hydroxyls (acidic/basic medium) is defined by two terms. The first related to the equilibrium of acids/bases of the reaction. The second considers the number of protons related to the formation of carbon dioxide (and other products, Table 1) as reaction products as well as the potential formation of carbonates from CO_2. Having information about the equilibrium constants of acid/bases as well as a number of pH measurements vs. time higher/equal to the number of chemical species, the resulting information can generate a linear set of equation. Solving this together with the atom/charge balances would allow to obtain the n_i parameters through a matrix inversion procedure combined with principal component analysis.[104]

The use of the S factor makes dramatic effects in the photonic yield and quantum efficiency observables. For example, in Figure 11 we present the case of gas-phase toluene and styrene photo-oxidation using a series of W-doped anatase samples. It can be seen that the two observables measured with/without selectivity provide different answers about the relative differences among samples and, in specific cases (toluene), about the trend through the sample series. The inclusion of chemical information in efficiency observables can thus give different information. It is not the same measuring the number of moles of reactant/products or the moles of charge carrier species utilized and thus the real number of photons generating chemical reactions per mole of (incident or absorbed) photons.

2.3.2. Global efficiency: from first principles to applied scale

The broad range of reactions and reactors utilized in photo-catalysis at any (lab, bench, pilot, industrial) scale requires a parameter that can measure the efficiency of the process at any scale level. Among different energetic parameters, the global efficiency parameter (η_T) is likely the most broadly utilized to facilitate the quantitative comparison between different photo-catalytic experiment conditions, reactor configurations and thus to determine reactor performances. The IUPAC defines this parameter as the ratio between useful (from a chemical point of view) and incoming energies.[16] The η_T can be defined, for electrical-energy driven systems, as the ratio between the number of reacting moles to the electrical power (P) necessary to operate the illumination source:

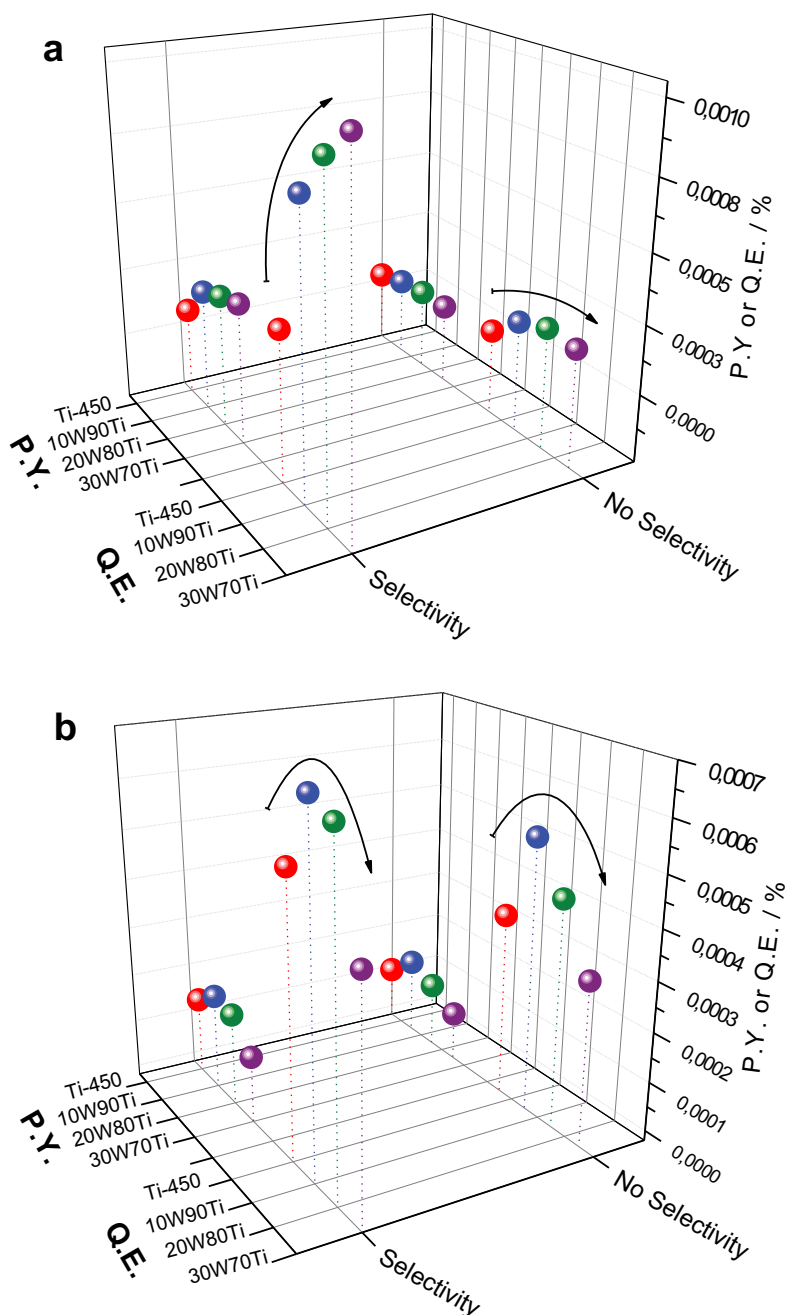$$\eta_T = \frac{reacting\ moles}{P} \qquad (11)$$

Figure 11. Photonic yield (P.Y.) and quantum efficiency (Q.E.) values for toluene (A) and styrene (B) photo-oxidation considering or not the selectivity of the reaction. Anatase (Ti-450) and W-doped anatase (xWyTi; with x:y the atomic composition on cation basis) powders were used as catalysts. Reproduced with permission from ref. 99. Copyright Elsevier.

One interesting general approach is to consider η_T (eq. 12) as the product of electrical efficiency (η_{ele}), incidence efficiency (η_{inc}), radiation absorption efficiency (η_{abs}) and reaction or quantum efficiency (η_q), each

observable can be expressed as an a-dimensional parameter, amenable for quantitative measurement, analysis and optimization.[106–108] Similarly, in the case of use solar-energy-driven systems, the η_T parameter could be defined as eq. 13.

$$\eta_T = \eta_{ele}\, \eta_{inc}\, \eta_{abs}\, \eta_q \qquad (12)$$

$$\eta_T = \eta_{inc}\, \eta_{abs}\, \eta_q \qquad (13)$$

The η_{ele} is the capacity of the radiation source to transform electrical energy into radiant energy (photons). In this sense, the most conventional sources used for the photo-catalyst activation are visible or UV lamps (incandescent and gas discharge) [14,109] However, these lamps render reduced conversion values of the electrical energy input into useful light, whereas the use of light-emitting diodes (LEDs) lamps offer a higher energy efficiency, longer lifetime and, in certain cases, a more flexible reactor design.[110,111] The η_{inc} is defined as the ratio between the photons that enter at the reactor to the photons provided by the illumination source.[112] The η_{abs} is a parameter that strongly depends of the optical properties of the catalysts since it is the ratio of the number of absorbed photons to the number of incident photons.[113] Figure 7 shows two typical situations for supported and suspended catalysts. The figure displays schematically the different light–matter interaction phenomena taking place in both cases and thus relevant for the calculation of η_{inc} and η_{abs}. Figure 7 is also relevant to define η_q parameter that relates the reacting moles per mol of photon absorbed by the catalyst or related definitions, as thoroughly described in section 2.3. Of course, some of these parameters can be calculated in a single procedure but the final result corresponds to equations 12/13 .[106–108] These equations own the inherent advantage of rendering adimensional parameters and potential to check the efficiency loss(es) taking place at each step in the journey from electrical or solar energy to the reaction products.

Other, less general ways of measuring the overall efficiency of a photo-catalytic process have been reported. We can mention the photo-catalytic thermodynamic efficiency factor (PTFE). For hydroxyl-triggered reactions, this parameter is based on thermodynamic considerations and defined as the ratio of the energy used for the formation of hydroxyl radicals to the energy absorbed by the catalyst.[114] Also, for hydrogen photo-production reactions, the "solar to hydrogen" parameter (STH) considers the ratio between the energy enclosed in the generated hydrogen product vs. the one of the incoming radiation flux.[115] These measurements are, in any case, less general and significantly less informative than equations 11–13.

2.4. *Kinetics: general analysis and interpretation of photo-activity*

The study of the kinetics of photo-catalytic reactions is here (this section) approached from the point of view of extracting information able to provide a quantitative ground for photo-activity assessment.

The ***first*** critical issue in this quest can be summarized in a simple phrasing saying that a kinetic analysis must be carried out rigorously. This task concerns (i) understanding the consequences of the local nature of the rate of photon absorption as well as the transfer problems customarily present in photo-catalytic processes (particularly when using suspended catalysts). As shown latter, the tradeoff between these two phenomena is a keystone in reactor design and scaling. These two issues together demand that hydrodynamic models, mass balances, and the radiation transport equation have to be simultaneously solved in each kinetic approach intended.[8,9,13,14] This central piece of photo-catalytic kinetic analysis as sketched in the core of Figure 12. Note also (ii) that the kinetic model would need to be of intrinsic type, based on the use of the rate of photon absorption observable to include rigorously light effects in photo-catalytic kinetic schemes. Finally, (iii) a complete scanning of all relevant (light and chemical-related) variables should be carried out. Adequate variables and experimental ranges can be obtained though a rational experimental design procedure. Making kinetic analysis without complying with all these requirements seems of little utility in the context of obtaining physico-chemical information for catalytic assessment.
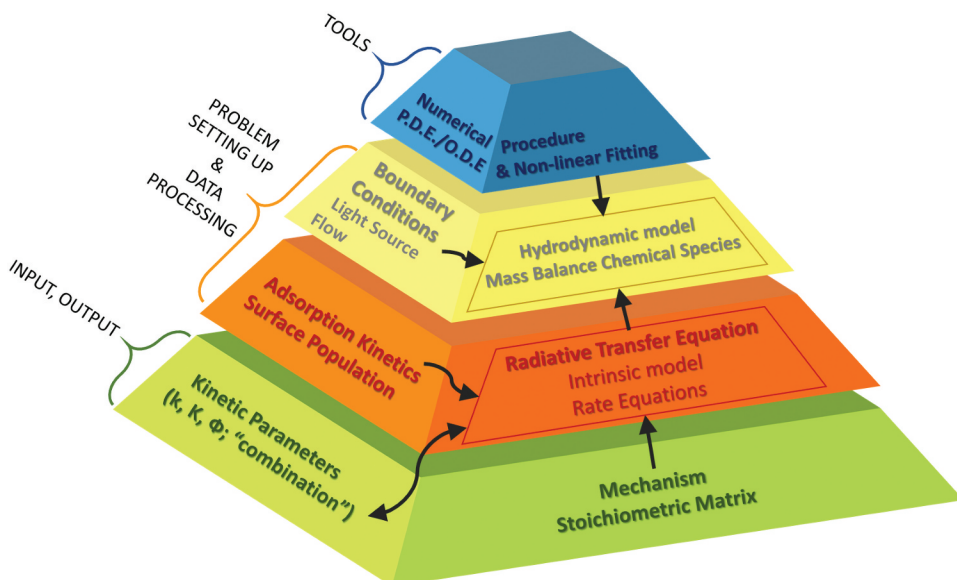
Figure 12. Schematic representation of a general kinetic approach in heterogeneous photo-catalysis. Symbols: k: rate constant(s); K: adsorption constant(s), Φ: primary quantum yield.

The point (i) of the above list is a complex task that we just briefly summarize here. For isothermal (Newtonian non-compressible) fluids having laminar flow, the modeling of the system includes the simultaneous resolution of the momentum, radiation transfer, and mass balances equations considering heterogeneous reactions as:

Continuity equation:

$$\underline{} \cdot \left(\rho \underline{\gamma} \right) = 0 \tag{14}$$

Momentum equation:

$$\underline{} \cdot \left(\rho \underline{\gamma}\underline{\gamma} \right) = -\underline{}P + \underline{} \cdot \left(\underline{\underline{\tau}} \right) + \rho \underline{g} \tag{15}$$

Species i conservation equation:

$$\underline{} \cdot \left(\rho \underline{\gamma} C_i \right) = \underline{} \cdot \underline{J_i} + R_i \tag{16}$$

Where ρ is the fluid density, $\underline{\gamma}$ is the velocity vector, P is the pressure, $\underline{\underline{\tau}}$ is the viscous stress tensor, $\underline{g}$ is the gravitational acceleration, C_i is the molar concentration of species I, $\underline{J_i}$ is the diffusion flux vector for species i, and R_i is the reaction rate of species i. The set of equations can be solved using computational fluid dynamics (CFD) considering the corresponding boundary fluid and illumination conditions (central part of Figure 12). Equation 16 concerns suspended (so-called pseudo-homogeneous) processes. For supported (so-called heterogeneous) processes the reaction rate appears in one boundary condition. In the case of simple geometries (annular, flat-plate wall reactors), a steady-state two-dimensional axial convention and radial (orthogonal) diffusion mass balance can be applied.[8,9,14] Continuous wall reactors correspond to the simplest case to model mathematically. This is usually carried out using the plug flow hypothesis and the species i conservation then becomes:

$$\langle \gamma_z \rangle \frac{\partial C_i}{\partial z} = a_\gamma R_i \tag{17}$$

Where a_γ is the ratio of catalytic area to reactor volume and z is the spatial coordinate representing the flow direction .[8] The set of equations calls for numerical procedures allowing to solving partial and/or ordinary differential equations (P.D.E. and O.D.E. acronyms, respectively, at the top of Figure 12). The computational problem corresponds to a non-linear fitting optimization using initial (guess) values for the parameters shown at the bottom row of Figure 12 and subjected to simultaneous solving of equations 14–16. Minimization of the error between experimental and model values of the reaction rate(s) leads to the final, optimized values of the kinetic parameters.

The **second** point is related to whether the kinetic model can or cannot provide information about the surface chemical steps of the reaction. In a broadly speaking way, this connects with the introduction paragraphs starting the discussion about the active center and whether such center can be formulated in an exact parallel way to heterogeneous catalysis. Photo-catalytic mechanisms are of radical nature and the study of the radical species combining spectroscopy and reaction rate(s) demonstrates that a quantitative relationship can be established. This has been the case for, mostly, $^{\bullet}$OH (hydroxyl) radical mediated mechanisms. For example, literature reports can be found for photo-degradation of 2-propanol, [116] acetaldehyde, [117,118] toluene [119,120] or hydrogen production from sacrificial alcohols.[121] Others utilized jointly bare holes and •OH species for toluene oxidation.[122] This clearly shows that, at least, surface information about the generation of reactive centers for kinetically relevant radicals is potentially available. In addition, kinetic isotope effects and microkinetic models from spectroscopic data confirm that chemical species are involved in kinetic relevant steps. Significant kinetic isotope effects have been detected in the oxidation of alcohols, [123] degradation of dyes, [124] hydrogen photo-production from alcohols, [125] or reduction of carbon dioxide with water.[126] Similarly, spectroscopic-based microkinetic analyses showing chemical species involved in kinetic-relevant steps have been presented for photo-degradation of 2-propanol, [127] acetaldehyde, [128] acetone, [129] and the photo-production of hydrogen.[130] While the above mentioned articles cannot provide a conclusive proof of a surface-type active center involved in a kinetically relevant chemical step as a general case, they certainly provide strong clues in this direction for a significant number of reactions and catalysts.

So, photo-catalytic kinetic formalisms can be derived from reaction mechanisms, which can include light rigorously (utilizing the rate of photon absorption) and can have a reasonable parallelism with those schemes typically utilized in heterogeneous catalysis. This is the framework required to derive the input information (e.g. mechanism) described at the bottom of Figure 12. Based in these premises, and considering the three main radical species (bare hole, hydroxyl and superoxide radicals) involved in heterogeneous photo-catalysis, [1–3,8,9,13–15] a general mechanism can have the steps included in Table 2. Note that the reaction mechanisms presented can be applied to oxidation reactions, the generation of hydrogen for sacrificial organic molecules (where the sacrificial molecule can suffer the attack of bare holes and/or hydroxyls) as well as the CO_2 reduction with water. The general mechanism considers charge regeneration, recombination, and capture by chemical species at surface and/or defects, and the subsequent reactions at the surface by target molecules or stable intermediates. Finally, a general step for radical de-activation (termination) is included.[8–10,13–15]

Table 2. General mechanism(s) of photo-catalytic reactions based on radical species. Symbols: k, rate constant; r_g rate of charge carrier generation; [] denotes the surface (subfix "ads") concentration of achemical or charge carrier species, Cat, catalyst; D, defect; X, target (reactant) molecule; Y, intermediate species; Z, product; and M, radical quencher.

reaction step	reaction rate	Eq. Number
Generation		
$Cat + \lambda\nu \xrightarrow{rg} Cat + h^+ + e^-$	r_g	(18)
Recombination		
$h^+ + e^- \xrightarrow{k_r} heat$	$k_r[h^+][e^-]$	(19)
Charge Capture and Trapping		
$e^- + O_{2\ ads} \xrightarrow{k_e} O_2^-$	$k_e[O_2]_{ads}[e^-]$	(20)
$h^+ + H_2O_{ads} \xrightarrow{k_{OH}} OH^{\cdot} + H^+$	$k_{OH}[H_2O]_{ads}[h^+]$	(21)
$h^+ + D \xrightarrow{k_{hD}} h_D^+$	$k_{hD}[h^+]$	(22)
Target molecule		
$X_{ads} + OH^{\cdot} \xrightarrow{k_{XOH}} Y_i$	$k_{XOH}[X]_{ads}[OH^{\cdot}]$	(23)
$X_{ads} + h^+ \xrightarrow{k_{Xh}} Y_i$	$k_{Xh}[X]_{ads}[h^+]$	(24)
$X_{ads} + h_D^+ \xrightarrow{k_{XhD}} Y_i$	$k_{XhD}[X]_{ads}[h^+]$	(25)
$X_{ads} + O_2^- \xrightarrow{k_{XO2}} Y_i$	$k_{XO_2}[X_i]_{ads}[OH^{\cdot}]$	(26)
Stable Intermediates		
$Y_{i,ads} + OH^{\cdot} \xrightarrow{k_{YiOH}} Z_i$	$k_{YiOH}[X]_{ads}[OH^{\cdot}]$	(27)
$Y_{i,ads} + h^+ \xrightarrow{k_{Yih}} Z_i$	$k_{Yih}[X]_{ads}[h^+]$	(28)
$Y_{i,ads} + h_D^+ \xrightarrow{k_{YihD}} Z_i$	$k_{YihD}[X]_{ads}[h^+]$	(29)
$Y_{iads} + O_2^- \xrightarrow{k_{YiO2}} Z_i$	$k_{YiO_2}[X_i]_{ads}[O_2^-]$	(30)
Termination of radicals		
$OH^{\cdot} + M \rightarrow Products$	$k_{TOH}[OH^{\cdot}][M]$	(31)
$h^+ + M \rightarrow Products$	$k_{Th}[h^+][M]$	(32)
$h_D^+ + M \rightarrow Products$	$k_{ThD}[h^+][M]$	(33)
$O_2^- + M \rightarrow Products$	$k_{TO_2}[O_2^-][M]$	(34)

In the table, Cat represents the catalyst, D are localized defects allowing bare hole capture and M are surface sites or even chemical species facilitating the termination of the radical species. Apart from considering the three main radical species, the table takes into account the possibility of the direct and indirect (the latter taking place through trapping at surface sites of the catalysts) type mechanism for hole radical attack (equations 24/25 for the attack to the target molecule).[9,13,14] Using Table 2 and selecting one adsorption formalism (normally a simple or competitive Langmuir-Hinshelwood saturation type), we can derive expression for the consumption of the target molecule and/or any stable intermediate (the R_i "term" in equations 16 and 17). The whole task has been summarized as the input information and the mathematical formulation of the reaction rate (the two bottom rows of Figure 12).

As previously discussed [9,13] and visually described in Figure 13, this usually lead to rate expression with target molecule functionalities described as; (i) basic or competitive Langmuir-Hinshelwood (L-H) saturation kinetics; (i) zero-order kinetic, and (iii) first-order kinetics. In addition, common reaction rate
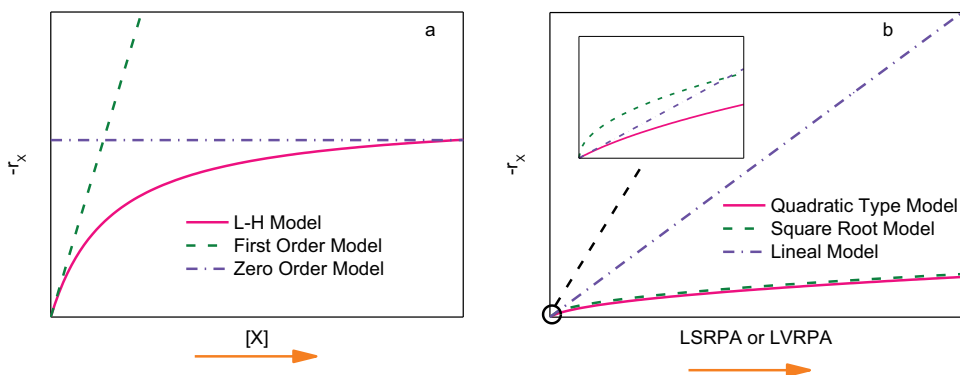
Figure 13. Reaction rate dependence (r_x) with the target molecule concentration [X] (A) and local (surface or volumetric. LSRPA or LVRPA) rate of photon adsorption (B). Other symbols: L-H Langmuir-Hinshelwood. Reprinted with permission from ref. 9. Copyright RSC.

dependences on the rate of photon absorption are: (i) quadratic-type; (ii) first order; and (iii) square root order. Specific models use variable order dependence going from 0.5 to 1 [131] or more complex expressions. [132]

As the (rate of photon adsorption) quadratic-type models can describe as limiting cases square-root and first-order type models (for respectively, high and low radiation flux limits), in Table 3 we displayed the analytical expression of the quadratic-type reaction rate of a target molecule and intermediates as a (reasonably) general formalism (no matter if the process makes use of suspended or supported catalysts). The mentioned asymptotic behavior of the

Table 3. Photo-catalytic reaction rate for the three main pathways of photo-catalytic reactions. Symbols: r_g: charge recombination rate defined in equation 18; k, rate constants for processes defined in Table 2; [] denotes the surface (subfix "ads") concentration of chemical or charge carrier species; X, target (reactant) molecule; Y, intermediate species; and M, radical quencher.

Mechanism type	Reaction rate	Eq. number
Hydroxyl	$$R_x = \frac{k_e k_{OH} k_{XOH}[H_2O_{ads}]\left[O_{2,ads}\right][X_{ads}]\left(1 - \frac{\sqrt{1+4k_r r_g}}{k_e k_{OH}[H_2O_{ads}]\left[O_{2,ads}\right]}\right)}{2k_r\left(k_{XOH}[X_{ads}] + \sum_i k_{YiOH}[Y_{i,ads}] + k_{TOH}[M]\right)}$$	(35)
	$$R_{y_i} = \frac{k_e k_{OH}\left(k_{YiOH}[Y_{i,ads}] - k_{XOH}[X_{ads}]\right)[H_2O_{ads}]\left[O_{2,ads}\right]\left(1 - \frac{\sqrt{1+4k_r r_g}}{k_e k_{OH}[H_2O_{ads}]\left[O_{2,ads}\right]}\right)}{2k_r\left(k_{XOH}[X_{ads}] + \sum_i k_{YiOH}[Y_{i,ads}] + k_{TOH}[M]\right)}$$	(36)
Hole	$$R_x = \frac{k_e k_{Xh}\left[O_{2,ads}\right][X_{ads}]\left(1 - \frac{\sqrt{1+4k_r r_g}}{k_e k_{Xh}[X_{ads}]\left[O_{2,ads}\right]}\right)}{2k_r}$$	(37)
	$$R_{y_i} = \frac{k_e\left(k_{Yih}[Y_{i,ads}] - k_{Xh}[X_{ads}]\right)\left[O_{2,ads}\right]\left(1 - \frac{\sqrt{1+4k_r r_g}}{k_e k_{Xh}[X_{ads}]\left[O_{2,ads}\right]}\right)}{2k_r}$$	(38)
Superoxide	$$R_x = \frac{k_e k_{OH} k_{XO_2}[H_2O_{ads}]\left[O_{2,ads}\right][X_{ads}]\left(1 - \frac{\sqrt{1+4k_r r_g}}{k_e k_{OH}[H_2O_{ads}]\left[O_{2,ads}\right]}\right)}{2k_r\left(k_{k_{XO_2}}[X_{ads}] + \sum_i k_{Y_iO_2}[Y_{i,ads}] + k_{TO_2}[M]\right)}$$	(39)
	$$R_{y_i} = \frac{k_e k_{OH}\left(k_{Y_iO_2}[Y_{i,ads}] - k_{Xk_{XO_2}}[X_{ads}]\right)[H_2O_{ads}]\left[O_{2,ads}\right]\left(1 - \frac{\sqrt{1+4k_r r_g}}{k_e k_{OH}[H_2O_{ads}]\left[O_{2,ads}\right]}\right)}{2k_r\left(k_{Xk_{XO_2}}[X_{ads}] + \sum_i k_{Y_iO_2}[Y_{i,ads}] + k_{TO_2}[M]\right)}$$	(40)

reaction rate vs. the irradiation flux has been shown to be universal (or at least dominant).[133] No adsorption/saturation formalism is included in order to maintain generality. The reaction rate expressions summarized in Table 3 are derived from the (corresponding radical) kinetic steps included in Table 2 (for the hole-radical mechanism we used equations 18/21/24/28/31) and utilized the steady state approximation for calculation of all radical species concentrations.

In Table 3, $r_g = \bar{\Phi}e^{a,s} or \frac{\bar{\Phi}}{a_\gamma} e^{a,s}$ for, respectively, supported and suspended catalysts, and $\bar{\Phi}$ is the primary quantum yield.[9] Note that for liquid phase, normally, the water concentration is a constant while for gas/liquid phase the oxygen concentration is constant as the use of air as oxygen source is frequently considered. Importantly, for (more or less) general expression such as those in Table 3 we cannot provide a full separation of chemical and light-related variables such as one presented in Figure 6. Nevertheless, there are important exceptions. For example, using the high irradiation flux limit and/or considering that recombination is much faster than any other reaction step, a square dependence of the rate of photon absorption (and independently of the chemical variable(s) dependence, as far as the ones described in Figure 13) is achieved and a full separation of variables is possible in all radical-mediated mechanisms presented in Table 3 .[9] A few linear dependent expressions typical of low irradiation flux schemes may also comply with this requirement. The specific conditions mentioned can justify a reaction rate analysis as presented in Figure 6. Thus, considering independent f(Cs) and g($\varphi \equiv e^a$) functions may be rigorous. Note that this requires the initial assessment of the g($\varphi \equiv e^a$) behavior vs. radiation flux prior studying f(Cs). Note also that this experimental procedure that does not require any computational work.

In any case, utilizing the rate expressions summarized in Table 3 and making use of a nonlinear fitting procedure, we can solve the set of (differential) equations 14 to 16 and obtain the kinetic parameter values. The goal of obtaining physico-chemical information from kinetic analysis is driven by the available information coming from the fitting parameters extracted from solving the general scheme presented in Figure 12. Unfortunately, we cannot access the individual values of the k_{xi} (i = OH·, h+, O$_2^-$) kinetic constants present in Table 2. This would require the combination of experimental and theoretical approaches, as customarily utilized in heterogeneous catalysis. However, the theoretical counterpart requires to setting-up nonadiabatic kinetic schemes over excited electronic states and only the initial stages of such procedures are currently available in the literature.[134,135] In photo-catalysis, we need to combine the different kinetic parameters (k_i: kinetic constants, K_i: adsorption constants,$\bar{\Phi}$ primary quantum yield) appearing in the equations of Table 3 in a series of constants, normally from 2 to 6.

Table 4 compiles frequently utilized mechanisms which can be used to extract experimental information. They correspond to general (liquid and gas phase) quadratic-type mechanisms considering hydroxyl, [136–139] hole [140,141] and

superoxide [9] radicals, gas-phase square-root-type mechanisms considering hydroxyl, [118–122,142] hole [122] and superoxide [9] radical species, and the so-called indirect/direct hole [143,144] and indirect disruptive hole [145,146] liquid-phase mechanisms. We note that there are other popular mechanisms summarized in literature reviews, which either do not fulfill the requirements above described or cannot render useful information in the context here scrutinized.[9,13,14] Also, in specific cases, the rate of photon absorption has been included in the fitting coefficients.[147]

From this table several physico-chemical pieces of information can be extracted. As a general rule, to extract information related to kinetic constants (k_{xi}) one should obtain (independently or within the fitting procedure) the values of the adsorption constants (K_i).

One general piece of information concerns the relationship between the kinetically relevant charge carrier species rates attacking the target molecule and the rate of charge recombination (equations 50,52,53) or the rate of termination of such radical species (equation 43,46,61). Analyzing the behavior of such observable though a series of catalysts (having similar composition, for example, analyzing the behavior of a titania-based system promoted with variable quantities of a metal or an oxide, etc.), it is possible to understand if the number of (surface) available radical species can dominate the chemical behavior of the reaction rate throughout the samples of the series. Bare hole radicals are unique in the context of the formalisms included in Table 4. Equation 45 only provides information about the primary quantum yield, while equation 56 informs about the ratio between rates of the hole attack to the target molecule vs. the formation (trough the utilization of "defects") of such radical species. In this last case, information about the hole attack to the target molecule would require to utilize the results from equations 56 and 58.

The second main information extracted from the kinetic study in presence of stable intermediates and/or co-products (the vast majority of photo-catalytic reactions) can be the ratio of kinetic constant for the radical attack to the target and stable intermediate(s) molecules (equations 44,47,51,54). Such a parameter would thus allow to interpret the selectivity of the reaction on physico-chemical basis. It would demonstrate whether kinetic or adsorption phenomena control selectivity.

Summarizing, rigorous kinetic approaches can render valuable information to assess photo-activity. First, they can prove the correct experimental conditions to study independently chemical and light-related variables and provide specific expressions for both of them. This provides a guide to utilize analytical procedures on rigorous bases (such as the one presented in Figure 6 for the reaction rate). Second, Table 4 collects information, which can rationalize the activity and selectivity of a photo-catalytic reaction. Because of the non-linear nature of the fitting process (Figure 12), it is complex to obtain "useful" values (in other words, with error values allowing the discern differences between

Table 4. Summary of physico-chemical information extracted from kinetic parameters. Kinetics formalisms are primarily defined by its dependence of the rate of photon absorption. Symbols: a_i constants defined from physico-chemical parameters; other symbols defined in Table 2.

Kinetic formalism
  Quadratic expression type. [a,b,c]

$$R_x = \frac{a_1[X_{ads}][H_2O_{ads}][O_{2,ads}]\left(1 - \frac{\sqrt{1+a_2r_g}}{[H_2O_{ads}][O_{2,ads}]}\right)}{\left(1 + a_3[X_{ads}] + \sum_i a_i[Y_{i,ads}]\right)} \tag{41}$$

$$R_y = \frac{\left(a_1[X_{ads}] - a_4[Y_{i,ads}]\right)[H_2O_{ads}][O_{2,ads}]\left(1 - \frac{\sqrt{1+a_2r_g}}{[H_2O_{ads}][O_{2,ads}]}\right)}{\left(1 + a_3[X_{ads}] + \sum_i a_i[Y_{i,ads}]\right)} \tag{42}$$

(a) Note that either water or oxygen concentration is a constant for, respectively, liquid or gas phase.
(b) Linear (low irradiation level; rate expression derived using a Taylor expansion for the square root term) and square root (high irradiation level; $a_2r_g \gg 1$) dependences of the rate of photon absorption leads to the same parameter relationships and information.
(c) For bare hole mechanism, the denominator becomes a constant introduced in a_1. See Eqs. 37,38.

OH$^.$ mechanism; useful combination of parameters. Refs [136–139]

$a_1\,a_2$	$\frac{k_{XOH}K_X}{k_{TOH}}\frac{2[sites]\Phi}{k_{XOH}K_X[M]}$	(43)
a_1/a_4	$\frac{k_{XOH}K_X}{k_{YiOH}K_{Y_i}}$	(44)

h$^+$ mechanism; useful combination of parameters. Refs [140,141]

$a_1\,a_2$	2Φ	(45)

O$_2^{.-}$. mechanism; useful combination of parameters. Refs [9]

$a_1\,a_2$	$\frac{k_{XO2}K_X}{k_{TO2}}\frac{2[sites]\Phi}{k_{XO2}K_X[M]}$	(46)
a_1/a_4	$\frac{k_{XO2}K_X}{k_{YiO2}K_{Y_i}}$	(47)

Kinetic formalism
  Square root dependence obtained assuming recombination rate much faster that any chemical step. Langmuir-Hinshelwood saturation kinetics. Gas phase. [a]

$$R_x = \frac{a_1[X][H_2O]\left(\sqrt{r_g}\right)}{\left(1 + K_{H2O}[H_2O] + K_X[X] + K_{Y_i}[Y_i]\right)\left(1 + K_{H2O}[H_2O] + K_X[X] + a_2[X] + \sum_i a_i[Y_{i,ads}]\right)} \tag{48}$$

$$R_y = \frac{\left(a_1[X] - a_4[Y_i]\right)[H_2O]\left(\sqrt{r_g}\right)}{\left(1 + K_{H2O}[H_2O] + K_X[X] + K_{Y_i}[Y_i]\right)\left(1 + K_{H2O}[H_2O] + K_X[X] + a_2[X] + \sum_i a_i[Y_{i,ads}]\right)} \tag{49}$$

(a) For bare hole mechanism the denominator is a constant introduced in a_1. For the superoxide mechanism, the first parenthesis of the denominator takes the value $(1 + K_{H2O}[H_2O])$.

OH$^.$ mechanism; useful combination of parameters. Refs . [118–120,142]

a_1/a_2	$\frac{k_{OH}K_{H2O}}{\sqrt{k_r}}[sites]\sqrt{\Phi}$	(50)
a_1/a_4	$\frac{k_{XOH}K_X}{k_{YiOH}K_{Y_i}}$	(51)

h$^+$ mechanism; useful combination of parameters. Refs . [122]

a_1	$\frac{k_{Xh}K_X}{\sqrt{k_r}}[sites]\sqrt{\Phi}$	(52)

O$_2^{.-}$ mechanism; useful combination of parameters. Refs . [9]

a_1/a_2	$\frac{k_{O2}K_{H2O}}{\sqrt{k_r}}[sites]\sqrt{\Phi}$	(53)
a_1/a_4	$\frac{k_{XO2}K_X}{k_{YiO2}K_{Y_i}}$	(54)

Kinetic formalism (hole only)
  Indirect/Direct hole Transfer model. Complex dependence. Langmuir-Hinshelwood saturation kinetics. Liquid phase. References . [143–145]

$$R_x = \frac{a_1a_2r_g[X]}{1+a_3[X]+a_2a_4[X]} + \left(\frac{a_4[X]+(1-a_5)a_6r_g[X]}{2a_4}\right)\left(\sqrt{1 + \left(\frac{a_4a_5a_6r_g}{(a_3[X]+(1-a_5)a_6r_g)^2}\right)} - 1\right) \tag{55}$$

a_1	$\frac{k_{Xh}}{k_{hD}}$	(56)
a_3	K_X	(57)
a_4	$k_{XhD}k_{O_2}[O_2]$	(58)
a_3	k_r	(59)

(Continued)

Table 4. (Continued).

Kinetic formalism (hole only)

Indirect hole "disruptive" model. Quadratic dependence. Langmuir-Hinshelwood saturation kinetics. Liquid phase. References .[13,146,147]

$$R_x = \frac{a_1[X]\left(-1 + \sqrt{1 + a_2 r_g}\right)}{(1 + a_3[X])} \tag{60}$$

$a_1\ a_2/\ a_3$

$$\frac{k_{XhD}}{k_{ThD}} \frac{2[sites]\Phi}{[M]} \tag{61}$$

---

samples or other situations) for the fitting coefficients. In this context, a critical issue relates to the point whether independent experimental information can (or cannot) be obtained in order to corroborate the kinetic model as well as the specific information(s) extracted from the above described analyses.

2.4.1. *Experimental validation of kinetic information*

Experimental validation of a photo-catalytic mechanism is a rather ambitious task and generally specking very complex. In most cases, the current status of the research field just leads to information to address specific aspects related to the involvement of the radical species into the mechanism and kinetics of the reaction. Also, using independent experimental information related to the adsorption constants and/or surface population of different chemical species we can test fitting consistency (and decrease error values of corresponding fitting parameters) or introduce such external information into the kinetic fitting process to extract specific information about kinetic constants.

In this context, the incorporation of specific (independently obtained) experimental information into kinetic schemes can be considered as the first important topic. We have previously mentioned a number of microkinetic studies using infrared spectroscopy and aiming to provide mechanistic and kinetic information of photo-catalytic reactions. These works mostly analyzed organic (particularly carbon-containing) moieties produced by interaction of the reactant and reaction intermediates with the catalysts and can render information about the surface coverage of the corresponding species.[127–130,148] As shown in Equations 35–40 and similar ones, information about water an oxygen species is also desirable. Under relevant (reaction) conditions, water can be studied using infrared spectroscopy but oxygen adsorption can be followed by several techniques. Superoxide radical species at the photo-catalyst surface can be directly (without the help of probe molecules) detected using vibrational (infrared and Raman) and electron paramagnetic resonance spectroscopies.[9,10,149,150] Alternative methods for oxygen (and other) radical species based in luminescent and other probe molecules and detection using optical spectroscopies are also available (although the chemical-catalytic effects of the probes are not always obvious).[9,10] Note, however, that combining classical (i.e., based in analytical
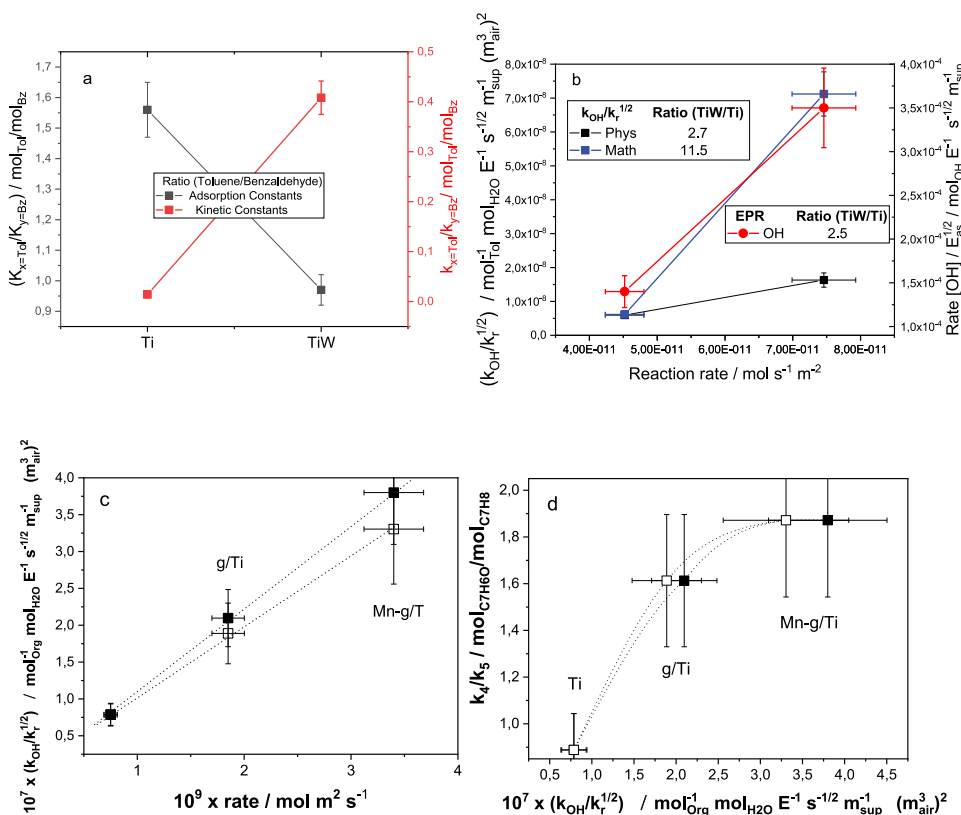
Figure 14. (A) Ratio between toluene (Tol) and benzaldehyde (Bz) adsorption and kinetic constants. ratio calculated using eq. 51 for the photo-degradation of toluene using anatase-titania (Ti) and tungsten oxide supported on Ti (TiW). (B) Ratio between kinetic constants for the chemical use of hydroxyl radical species and recombination vs. reaction rate of toluene photo-degradation. Ratio calculated with eq. 50 using experimentally independent kinetic schemes and spectroscopic (electron paramagnetic resonance, EPR) data. The insets show the ratio of the observables between TiW and Ti samples. see text for details. Reported from ref. 153. copyright Elsevier. (C) ratio between kinetic constants for the chemical use of hydroxyl radical species and recombination vs. reaction rate of toluene photo-degradation. ratio calculated with eq. 47 using a kinetic scheme and anatase-titania (Ti) and carbon nitride (g; promoted or not with MnOx, denoted as Mn in the graph) supported in Ti (g/Ti) samples. (D) correlation plot between the ratio of kinetic constants for toluene/benzaldehyde and the ratio between the chemical use of hydroxyl radical species and the recombination of charge. see text for details. Reported from ref. 152. copyright Elsevier.

methods to obtain reactant/product concentrations) chemical kinetic and (the above mentioned) spectroscopic approaches to feed (rigorous) intrinsic kinetic studies with surface-coverage data of reactants/intermediates/products is, to our knowledge, scarcely applied in the literature of the photocatalysis field.[9]

More broadly applied in photo-catalysis appears the incorporation of adsorption constant values into classical kinetic schemes. This can have a dual aim. First, it can render adequate conditions to decrease (fitting) error and, therefore, to choose the more appropriate (numerical) approximations to solve the "full" (equations 14 to 16) kinetic formalism.[151] Second, such adsorption constants

can be used to extract the value of kinetic constants according to equations 43, 44, 47, 50, 51, 54, 58, 152 and 153.[43,44,47,50,51,54,58,152,153] An example of application using the photo-oxidation of toluene is presented in Figure 14 (panel A). The mentioned degradation reaction generates benzaldehyde and carbon dioxide as products over two catalysts, a titania reference (Ti) and another having tungsten oxide supported in the mentioned reference (TiW). Figure 14A displays a comparison of the ratio between the adsorption and kinetic constants of toluene (the reactant) and benzaldehyde (the only stable intermediate in the way to carbon dioxide), for two catalysts. Opposite trends are observed when going from Ti to TiW. Quantitative analysis probes changes in surface properties but highlights a "dominant" kinetic origin of changes in selectivity when the tungsten component is incorporated over the titania reference.[153] As described in the previous subsection for this type of analysis, the effect of light on adsorption constants should be carefully considered.

As summarized in Table 4 the kinetic analysis of the fitting parameters can also render information about the ratio between the chemical use of kinetically relevant radical species and the involvement of such species in the recombination step. It can thus give a quantitative measurement of the chemical efficiency (involvement in the photo-catalytic reaction) of such radical species. This information can be useful in several ways.[118–120,142,152,153] Figure 14B plots such observable obtained using independent kinetic and spectroscopic ways of measuring the hydroxyl radical species generated using Ti and TiW catalysts and utilized for toluene photo-degradation. The activity (reaction rate; OX scale in the figure) increases for Ti to the TiW sample. This also occurs in the measurement of the OH⋅ radical species attacking the toluene (kinetic measurement) or the normalized (considering optical properties) rate of OH⋅ formation (EPR measurement). In first place, the positive (to be linear in the case for 2, trivial case, or more samples [118–120,142]) correlation between OH-related information and reaction rate using two independent measurements proves without doubt that the OH⋅ radical is the (only) kinetically relevant radical species, triggering the oxidation of the molecule. On second place, the analysis of different kinetic approaches (called "phys" and "math" in Figure 14B and differing in the fact that they include or not, respectively, relationships between the parameters to provide or not "physical" meaning), which can be hardly differentiated using error analysis, can be contrasted with the EPR measurement. This allows to select the adequate numerical/physical approximation(s) to solve the complex kinetic schemes always required in photo-catalysis.[153] A similar study to analyze the charge handling effects of the interface between (promoted or not with Mn) graphitic carbon nitride and titania is presented in Figure 14C. The plot shows that activity enhancement with respect to the parent titania is directly related to the balance achieved between hydroxyl radical species generation and recombination, again demonstrating that it is the kinetically relevant radical species. Finally, in

this carbon nitride – titania composite system, the simultaneous (kinetic) analysis of the activity and selectivity catalytic properties is displayed in Figure 14D. According to the authors, the study points out that presence of oxidized Mn species on the carbon nitride component alters significantly activity mostly affecting initial steps of the reaction but not those taking place after generation of benzaldehyde.[152]

3. Summary and outlook into the future

Assessment of photo-activity appears as a central piece to secure the correct future evolution of the photo-catalysis field. The contribution attempts to settle-down and discuss the current state of the art of the knowledge in the field considering two fundamental aspects, the measurement and the interpretation of the relevant observables. In this quest, we make an exhaustive analysis of the all relevant contributions, focussing attention in presenting a concise set of main guidelines for the *quantitative* assessment of photoactivity.

As well known, any catalytic reaction is characterized by its thermodynamic and kinetic parameters. For photo-catalysis the complete knowledge and understanding of these parameters is, however, hindered by the essential lack of information concerning the active center from all (structural/electronic and kinetic) perspectives. This is a general fact for all photo-catalytic reactions and has direct implications in the assessment of photo-activity at any (lab, pilot, industrial) scale. In spite of this problem, the current status of the field provides the basis for the quantitative assessment of photo-activity. This is currently carried out using a series of different "families" of parameters. The first family is the reaction rate and closely connected observables as the turnover frequency and number. The second corresponds to efficiency observables, going from the photonic yield and quantum efficiency of the reaction to the global efficiency of the process. The third family is related to the information enclosed in the kinetic constants derived from mechanistic-kinetic studies.

For all of them, key yet open (e.g. subjected to active research) questions are; (i) securing the report of data free of limitations and, particularly, not affected by the specific (experimental) conditions of the experiment and (ii), once the previous condition is met, how to extract all possible information from catalytic observables. A simple analysis of transport phenomena inherent to photo-catalysis showed a more complex situation than the one typically encountered in conventional catalysis. The interplay between mass and momentum transport together with radiative transfer phenomena (summarized in Figure 12 along a schematic representation of the procedure to tackle the problem) was analyzed in first place to discuss the adequate experimental conditions to handle transport effects or the exact mathematical procedures to

handle them. In this context, the review highlights that equations 14–16 (or equivalent ones) are at the core of the analysis and understanding of photo-catalytic reactions.

The reaction rate is the most broadly used observable to assess photo-activity. This parameter is a function of two types of variables, chemical (similar to thermal catalysis and described by the concentration of chemical entities) and light-related (obviously exclusive of photo-catalysis and inherently described by the primary quantum yield and the rate of photon absorption observables) ones. Both types of observables need to be considered in order to interpret activity-assessment results using reaction rates. The review shows that, in general, they are interrelated in a complex way. Yet in specific experimental conditions they can be independently studied. Restraining the measurements to regions where the reaction rate dependence on the rate of photon absorption shows a square-root dependence (high irradiation level) ensures the feasibility of the separation of variables between chemical and light-related ones in common radical (hydroxyl/hole/superoxide) photo-catalytic mechanisms. So, in such conditions the extraction of information from chemical variables or light alone is fully consistent and trustful and both can be coupled by a simple multiplication (Figure 6) to fully describe the reaction rate behavior. In the remaining cases, a full experimental design of chemical and light-related dependence of the reaction rate must be afforded in order to present a meaningful comparison between catalytic systems. The use of correct experimental design and statistical analytical tools are required to provide information in such cases. Table 4 summarizes some of the (up to date) general and broadly applied analytical expressions for the photo-catalytic reaction rates. To end with this family of activity-assessing parameters, it appears obvious that the limited knowledge about the active center strongly limits the usefulness of any report based in the turnover concept. Nevertheless, the progress along this line is most desired. Although out of the scope of this review, unravelling the (geometrical/electronic) structure of the reaction active center within a kinetic/mechanistic context would require new theoretical and experimental (characterization) techniques among which "single particle" – "single event" as well as advanced and time-resolved (vibrational, optical, etc.) spectroscopies and time-dependent DFT studies would contribute significantly to generate the desired new information.

Efficiency is the general parameter recommended by the IUPAC to assess photo-activity at any application level, from laboratory to industry. The review detailed how the photonic yield or quantum efficiency observables can be measured and computed for any photo-catalytic reaction using suspended or supported catalysts. The "dimensionality" of the efficiency observable(s) as well as the weakness related to "void" volume (also called dead volume or shadowing) effects were discussed in detail. In brief, the current situation is that the procedure(s) to achieve rather accurate calculations of the photonic yield and,

particularly, quantum efficiency is (are) well known, albeit they are scarcely followed as they require intensive and time-consuming experimental and computational procedures. From the dimensionless quantum efficiency (or closely related definitions), the global efficiency of a photo-catalytic process can be calculated. The global efficiency (equations 10–13) is the parameter to analyze and compare the performance of any catalyst at any (lab, pilot, industrial) scale and is thus a central piece to judge photo-activity in a general context. The parameter gives a true measurement of the energetic efficiency (or balance) of the photo-catalytic process. Moreover, the detailed knowledge of its components renders full information to compare in a quantitative way photo-catalytic processes carried out at different experimental conditions (light sources, substrate, operation conditions, etc.) and scale.

The third family to assess photo-activity is connected with the information extracted from kinetic formalisms. The kinetic formalism for any photo-catalytic reaction requires the usage of the rate of photon absorption in order to measure quantitatively the light-dependence of the rate of appearance or disappearance of any molecule. This leads to the so-called "intrinsic" kinetic formalisms. Unfortunately, the inherent complexity of photo-catalytic mechanisms, the stringent experimental conditions necessary for a meaninful interrogation of catalysts under illumination, as well as the limited support from theoretical tools make the knowledge of kinetic constants of relevant kinetic steps unfeasible.
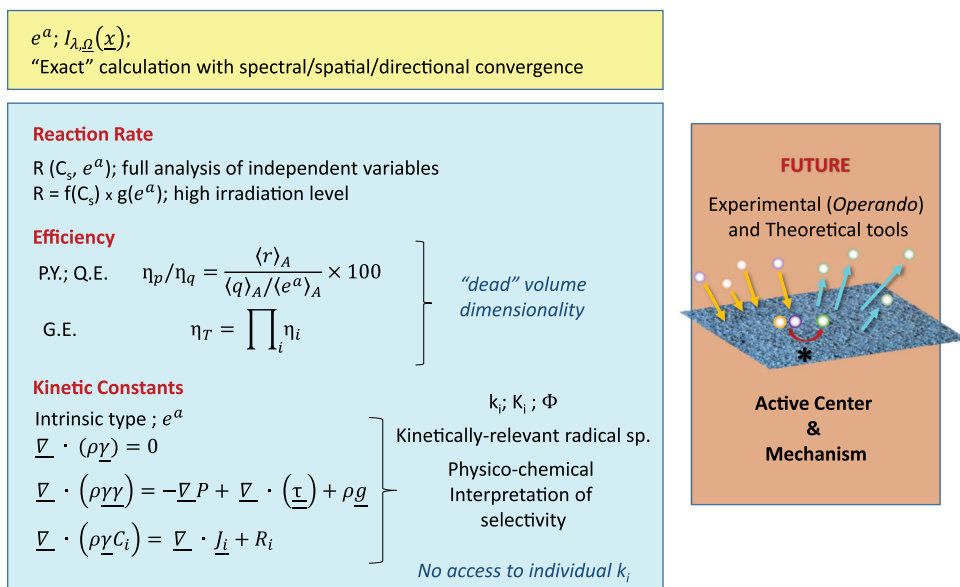
Figure 15. Schematic representation of photo-catalytic observables, key concepts in present procedures for measurement/calculation, and current and future challenging issues. Acronysms: P.Y. Photonic yield; Q.E. Quantum efficiency; G.E. Global Efficiency. See text for symbol meaning and details.

Thus, rather than specific kinetic constant values, the current state of the art provides numerical information about parameters with functional dependence of kinetic and adsorption constants as well as the primary quantum yield. In the case of mechanisms dominated by hydroxyl/holes/superoxide radicals (the majority of the previously reported in the literature), these parameters can be used to analyze on quantitative basis the performance of a catalyst along a series of samples. Specifically, independently of the reaction mechanism of the reaction, information can be obtained about the nature and number of charge carriers reaching the surface of a catalyst and involved in chemical species with respect to those recombining. Also, exploiting the analysis of selectivity of the photo-catalytic reaction, we can obtain a relationship between the kinetic constants of the radical attack to the target, initial molecule, and any stable intermediate. The review shows how the mentioned information(s) can be confronted with spectroscopic studies. In this way, using the overall kinetic analysis, the type of radical species involved in kinetically relevant steps can be unveiled. In addition, the (possible) kinetic control of the reaction products (selectivity) can be validated and quantified. The latter is particularly important to understand the physico-chemical control of selective reactions like partial oxidation or reduction processes, or the potential ways to drive selectivity in complex reactions like CO_2 reduction.

Figure 15 summarizes the main findings of this contribution. Due to the inherent complexity of the light–matter interaction taking place under a photo-catalytic reaction, the measurement, analysis, and interpretation of the corresponding (catalytic) observables is significantly more complex than in conventional catalysis. However, the rigorous bases to carry out such task(s) are clearly established, and general procedures to obtain exact and robust values for assessing photo-activity are in place and available to the researchers. This particularly concerns the calculation of the photon rate of absorption as a central tool in this quest (a yellow box highlights this issue in Figure 15). Both the key issues/formulas/procedures for obtaining the observables and remaining challenging points (highlighted using blue letters) have been summarized in this section and are schematically presented in the green-blue box of Figure 15. Moreover, significant advancement in the research field, particularly (i) to define the active center of the reaction and photo-catalytic mechanisms, and (ii) to introduce novel (from operando spectrocopies and TD-DFT) information in kinetics schemes (red box in Figure 15), can be achieved in the near future and must pave the way for improving our current understanding of photo-catalysis through critical contributions to the assessment of photo-activity, a central stone of the photo-catalytic field.

Acknowledgments

Disclosure statement

No potential conflict of interest was reported by the author(s).

References

[1] Kubacka, A.; Fernández-García, M.; Colón, G. Advanced Nanoarchitectures for Solar Photocatalytic Applications. *Chem. Rev.* 2012, *112*(3), 1555–1614. DOI: 10.1021/cr100454n.

[2] Colmenares, J.C., and Luque, R. Heterogeneous Photocatalytic Nanomaterials: Prospects and Challenges in Selective Transformations of biomass-derived Compounds *Chem. Soc. Rev.* 2014, *43*(3), 765–778. DOI: 10.1039/C3CS60262A.

[3] Teixeira, I.F.; Barbosa, E.C.M.; Tang, S.C.E., and Camargo, P.H.C. Carbon Nitrides and Metal Nanoparticles: From Controlled Synthesis to Design Principles for Improved Photocatalysis. *Chem. Soc. Rev.* 2018, *47*(20), 7783–7817. DOI: 10.1039/C8CS00479J.

[4] Chen, Q.; Shen, C.; He, L. Recent Advances of polyoxometalate-catalyzed Selective Oxidation Based on Structural Classification. *Act. Crys.* 2018, *C 74*, 1182–1201. DOI: 10.1107/S2053229618010902.

[5] Yu, H.; Jiang, L.; Wang, H.; Huang, B.; Yuan, X.; Huang, J.; Zhang, J.; Zeng, G. Modulation of Bi2MoO6-Based Materials for Photocatalytic Water Splitting and Environmental Application: A Critical Review. *Small.* 2019, *15*, 1901008. DOI: 10.1002/smll.201901008.

[6] Kubacka, A.; Caudillo-Flores, U.; Barba-Nieto, I., and Fernández-García, M. *Appl. Catal. A: General*; 2021; Vol. 610, pp 117966. DOI: 10.1016/j.apcata.2020.117966.

[7] Serpone, N. Relative Photonic Efficiencies and Quantum Yields in Heterogeneous Photocatalysis. *J. Photochem. Photobiol. A Chem.* 1997, *104*(1–3), 1–12. DOI: 10.1016/S1010-6030(96)04538-8.

[8] Cassano, A.E., and Alfano, O.M. Reaction Engineering of Suspended Solid Heterogeneous Photocatalytic Reactors. *Catal. Today.* 2000, *58*(2–3), 167–197. DOI: 10.1016/S0920-5861(00)00251-0.

[9] Muñoz-Batista, M.J.; Ballari, M.M.; Kubacka, A.; Alfano, O.M., and Fernández-García, M. Braiding Kinetics and Spectroscopy in photo-catalysis: The spectro-kinetic Approach. *Chem. Soc. Rev.* 2019, *48*(2), 637–682. DOI: 10.1039/C8CS00108A.

[10] Nosaka, Y., and Nosaka, A.Y. Generation and Detection of Reactive Oxygen Species in Photocatalysis. *Chem. Rev.* 2017, *117*(17), 11302–11336. DOI: 10.1021/acs.chemrev.7b00161.

[11] Ohtani, B. Revisiting the Fundamental Physical Chemistry in Heterogeneous Photocatalysis: Its Thermodynamics and Kinetics. *Phys. Chem. Chem. Phys.* 2014, *16* (5), 1788–1797. DOI: 10.1039/c3cp53653j.

[12] Liu, B.; Zhao, X.; Terashima, C.; Fujishima, A.; Nakata, K. Thermodynamic and Kinetic Analysis of Heterogeneous Photocatalysis for Semiconductor Systems. *Phys. Chem. Chem. Phys.* 2014, *16*(19), 8751–8760. DOI: 10.1039/c3cp55317e.

[13] Mills, A.; O´Rouke, C., and Moore, K. Powder Semiconductor Photocatalysts in Aqueous Solution: An Overview of kinetic-based Reaction Mechansims. *J. Photochem. Photobiol. A.* 2015, *310*, 66–105. DOI: 10.1016/j.jphotochem.2015.04.011.

[14] Boyjoo, Y.; Sun, H.; Liu, J.; Pareek, V.K., and Wang, S. A Review on Photocatalysis for Air Treatment: From Catalyst Development to Reactor Design. *Chem. Eng. J.* 2017, *310*, 537–559. DOI: 10.1016/j.cej.2016.06.090.

[15] Ollis, D.F. Kinetic Disguises in Heterogeneous Photocatalysis. *Top. Catal.* 2005, *35*(3–4), 217–223. DOI: 10.1007/s11244-005-3827-z.

[16] Braslavsky, S.E.; Braun, A.M.; Cassano, A.E.; Emeline, A.V.; Litter, M.I.; Palmisano, L.; Parmon, V.N., and Serpone, N. Glossary of Terms Used in Photocatalysis and Radiation Catalysis (IUPAC Recommendations 2011). *Pure Appl. Chem.* 2011, *83*(4), 931–1014. DOI: 10.1351/PAC-REC-09-09-36.

[17] Muñoz-Batista, M.J.; Caudillo-Flores, U.; Ung-Medina, F.; Chaez-Parga, M.C.; Cortés, J. A.; Kubacka, A., and Fernández-Garcia, M. Gas Phase 2-Propanol Degradation Using Titania Photocatalysts: Study of the Quantum Efficiency. *Appl. Catal. B.* 2017, *201*, 400–410. DOI: 10.1016/j.apcatb.2016.08.014.

[18] Van Gerven, T.; Mul, G.; Moulijn, J.; Stankiewicz, A. A Review of Intensification of Photocatalytic Processes. *Chem. Eng. Process. Process. Intensif.* 2007, *46*(9), 781–789. DOI: 10.1016/j.cep.2007.05.012.

[19] Zhong, L.; Haghighat, F. Photocatalytic Air Cleaners and Materials Technologies - Abilities and Limitations. *Build. Environ.* 2015, *91*, 191–203. DOI: 10.1016/j.buildenv.2015.01.033.

[20] Ballari, M.M.; Brandi, R.; Alfano, O., and Cassano, A. Mass Transfer Limitations in Photocatalytic Reactors Employing Titanium Dioxide Suspensions. I. Concentration Profiles in the Bulk. *Chem. Eng. J.* 2008, *136*(1), 50–65. DOI: 10.1016/j.cej.2007.03.028.

[21] Klaewkla, R.; Arend, M.G., and Hoelderich, W. A Review of Mass Transfer Controlling the Reaction Rate in Heterogeneous Catalytic Systems. *Mass Transfer - Advanced Aspects, InTech.* 2011. DOI: 10.5772/22962.

[22] Mehrotra, K.; Yablonsky, G.S., and Ray, A.K. Kinetic Studies of Photocatalytic Degradation in a TiO$_2$ Slurry System: Distinguishing Working Regimes and Determining Rate Dependences. *Ind. Eng. Chem. Res.* 2003, 42, 2273–2281. DOI: 10.1021/ie0209881.

[23] Ballari, M.M.; Alfano, O.M., and Cassano, A.E. Mass Transfer Limitations in Slurry Photocatalytic Reactors: Experimental Validation. *Chem. Eng. Sci.* 2010, *65*(17), 4931–4942. DOI: 10.1016/j.ces.2010.04.021.

[24] Kapteijn, F.; Moulijn, J. A. *Handbook of Heterogeneous Catalysis*, 2nd ed.; Ertl, G., Knozinger, H., Schuth, F., Weitkamp, J., Eds; Wiley-VCH: Weinheim, 2008; pp. 2019–2045.

[25] Kramm, U.I.; Marschall, R., and Rose, M. Pitfalls in Heterogeneous Thermal, Electro- and Photocatalysis. *ChemCatChem.* 2019, *11*(11), 1–13. DOI: 10.1002/cctc.201900137.

[26] Kubacka, A.; Barba-Nieto, I.; Caudillo-Flores, U.; Fernández-García, M. Interpreting quantum Efficiency for Energy and Environmental Applications of photo-catalytic Materials. *Curr. Op. Chem. Eng.* 2021, *33*, 100712. DOI: 10.1016/j.coche.2021.100712.

[27] Ohtani, B. Preparing Articles on Photocatalysis—Beyond the Illusions, Misconceptions, and Speculation. *Chem. Lett.* 2008, *37*(3), 216–229. DOI: 10.1246/cl.2008.216.

[28] Kisch, H.; Bahnemann, D. Best Practice in Photocatalysis: Comparing Rates or Apparent Quantum Yields? *J. Phys. Chem. Lett.* 2015, *6*(10), 1907–1910. DOI: 10.1021/acs.jpclett.5b00521.

[29] Qureshi, M.; Tanabe, K. Insights on Measuring and Reporting Heterogeneous Photocatalysis: Efficiency Definitions and Setup Examples. *Chem. Mater.* 2017, *29*(1), 158–167. DOI: 10.1021/acs.chemmater.6b02907.

[30] Melchionna, M.; Fornasiero, P. Updates on the Roadmap for Photocatalysis. *ACS Catal.* 2020, *10*(10), 5493–5501. DOI: 10.1021/acscatal.0c01204.

[31] Vignolo-González, H.A.; Laha, S.; Jiménez-Solano, A.; Oshima, T.; Duppel, V.; Schutzenbude, P., and Lotsch, B.V. Toward Standardized Photocatalytic Oxygen Evolution Rates Using RuO_2@TiO_2 as a Benchmark. *Matter.* 2020, *3*(2), 464–486. DOI: 10.1016/j.matt.2020.07.021.

[32] Burwell, R.L. Manual of Symbols and Terminology for Physicochemical Quantities and Units - Appendix II. Definitions, Terminology and Symbols in Colloid and Surface Chemistry. Part II: Heterogeneous Catalysis. *Pure Appl. Chem.* 1976, *46*, 7190. DOI: 10.1351/pac197646010071.

[33] Eaton, T.R.; Campos, M.P.; Gray, K.A., and Notestein, J.M. Quantifying Accessible Sites and Reactivity on titania-silica (Photo) Catalysts: Refining TOF Calculations. *J. Catal.* 2014, *309*, 156–165. DOI: 10.1016/j.jcat.2013.09.015.

[34] Simpson, B.H., and Rodríguez-López, J. Redox Titrations via Surface Interrogation Scanning Electrochemical Microscopy at an Extended Semiconducting Surface for the Quantification of Photogenerated Adsorbed Intermediates. *Electrochim. Acta.* 2015, *179*, 74–83. DOI: 10.1016/j.electacta.2015.04.128.

[35] Luo, C.; Ren, X.; Dai, Z.; Zhang, Y.; Qi, X.; Pan, C. Present Perspectives of Advanced Characterization Techniques in TiO_2-based Photocatalysts. *ACS Appl. Mater. Interfaces.* 2017, *9*(28), 23265–23286. DOI: 10.1021/acsami.7b00496.

[36] Caudillo-Flores, U.; Muñoz-Batista, M.J.; Kubacka, A., and Fernández-García, M. Operando Spectroscopy in Photocatalysis. *ChemPhotoChem.* 2018, *2*(9), 777–785. DOI: 10.1002/cptc.201800117.

[37] Muñoz-Batista, M.J.; Motta-Meira, D.; Colón, G.; Kubacka, A., and Fernández-García, M. Phase-Contact Engineering in Mono- and Bimetallic Cu-Ni Co-catalysts for Hydrogen Photocatalytic Materials. *Angew. Chem. Int. Ed.* 2018, *57*(5), 1199–1203. DOI: 10.1002/anie.201709552.

[38] Caudillo-Flores, U.; Barba-Nieto, I.; Muñoz-Batista, M.J.; Kubacka, A., and Fernández-García, M. Characterization of Photo-catalysts: From Traditional to Advanced Approaches. *Topics Curr. Chem.* 2019, *24*, 377–399. DOI: 10.1007/s41061-019-0248-1.

[39] Fontelles-Carceller, O.; Muñoz-Batista, M.J.; Conesa, J.C.; Fernández-García, M., and Kubacka, A. UV and Visible Hydrogen photo-production Using Pt Promoted Nb-doped TiO_2 photo-catalysts: Interpreting Quantum Efficiency. *Appl. Catal. B.* 2017, *216*, 133–145. DOI: 10.1016/j.apcatb.2017.05.022.

[40] Ray, S.; Lalman, J.A., and Biswas, N. Using the Box-Benkhen Technique to Statistically Model Phenol Photocatalytic Degradation by Titanium Dioxide Nanoparticles. *Chem. Eng. J.* 2009, *150*(1), 15–24. DOI: 10.1016/j.cej.2008.11.039.

[41] García, B.B.; Lourinho, G.; Romano, P., and Brito, P.S.D. Photocatalytic Degradation of Swine Wastewater on Aqueous TiO_2 Suspensions: Optimization and Modeling via Box-Behnken Design. *Helyon.* 2020, *6*(1), e03293. DOI: 10.1016/j.heliyon.2020.e03293.

[42] ISO (International Organization for Standardization) (2016). ISO 22197-1. Fine Ceramics (Advanced Ceramics, Advanced Technical Ceramics)-Test Method for Air-Purification Performance of Semiconducting Photocatalytic Materials-Part 1: Removal of Nitric Oxide. https://www.iso.org/standard/65416.html.

[43] ISO (International Organization for Standardization) (2019). ISO 22197-2. Fine Ceramics (Advanced Ceramics, Advanced Technical Ceramics)-Test Method for Air-Purification Performance of Semiconducting Photocatalytic Materials-Part 2: Removal of Acetaldehyde https://www.iso.org/standard/72347.html.

[44] Baumanis, C., and Bahnemann, D.W. TiO$_2$ Thin Film Electrodes: Correlation between Photocatalytic Activity and Electrochemical Properties. *J. Phys. Chem. C.* 2008, *112*(48), 19097–19101. DOI: 10.1021/jp807655a.

[45] Khan, A.; Goepel, M.; Kubas, A.; Lomot, D.; Lisowski, W.; Lisovytskiy, D.; Nowicka, A.; Colmenares, J.A., and Glaser, R. Slective Oxidation of 5-Hydromehylfurfural to 2,5-Diformylfuran by Visible Light-driven Photocatalysis over in-situ substrate-sensitized Titania. *ChemSusChem.* 2021, *14*(5), 1351–1362. DOI: 10.1002/cssc.202002687.

[46] Mills, A.; Hill, C., and Robertson, P.K. Overview of the Current ISO Tests for Photocatalytic Materials. *J. Photochem. Photobiol.* 2012, *237*, 7–23. DOI: 10.1016/j.jphotochem.2012.02.024.

[47] Satuf, M.L.; Brandi, R.J.; Cassano, A.E., and Alfano, O.M. Experimental Method to Evaluate the Optical Properties of Aqueous Titanium Dioxide Suspensions. *Ind. Eng. Chem. Res.* 2005, *44*(17), 6643–6649. DOI: 10.1021/ie050365y.

[48] Du, Y.; Liu, M.; Gou, L. Scattering Phase Function of Fractal Aggregates of TiO$_2$ Particulate Photocatalyst Simulated with Discrete Dipole Approximation. *Int. J. Hydrogen Energ.* 2020, *45*(52), 28034–28043. DOI: 10.1016/j.ijhydene.2020.03.223.

[49] García-Gil, A.; Casado, C.; Pablos, C.; Marugán, J. Novel Procedure for the Numerical Simulation of Solar Water Disinfection Processes in Flow Reactors. *Chem. Eng. J.* 2019, *376*, 120194. DOI: 10.1016/j.cej.2018.10.131.

[50] Caudilllo-Flores, U.; Agostini, G.; Marini, C.; Kubacka, A.; Fernández-García, M. Hydrogen thermo-photo Production Using Ru/TiO$_2$: Heat and Light Synergistic Effects. *Appl. Catal. B.* 2019, *256*, 117790. DOI: 10.1016/j.apcatb.2019.117790.

[51] Parrino, F.; Loddo, V.; Augugliaro, V.; Camera-Roda, G.; Plamisano, G.; Palmisano, L.; , and Yurdakal, S. S.Heterogeneous Photocatalysis: Guidelines on Experimental Setup, Catalyst Characterization, Interpretation, and Assessment of Reactivity. *Catal. Rev. Sci. Eng.* 2019, *61*(2), 163–213. DOI: 10.1080/01614940.2018.1546445.

[52] Casado, C.; García-Gil, A.; van Grieken, R.; Marugán, J. Critical Role of the Light Spectrum on the Simulation of Solar Photocatalytic Reactors. *Appl. Catal. B.* 2019, *252*, 1–9. DOI: 10.1016/j.apcatb.2019.04.004.

[53] Ramos-Huerta, L.A.; Valadés-Pelayo, P.J.; Llanos, A.G.; Ruiz, R.S.; Cabello, J.J., and Castillo-Araiza, C.O. Development of a New Methodology to Determine Suspended Photocatalyst Optical Properties. *Chem. Eng. J.* 2021, *413*, 127458. DOI: 10.1016/j.cej.2020.127458.

[54] Pellegrino, F.; Pellutie, L.; Sordelo, F.; Minero, C.; Ortel, E.; Hodoraba, V.-D.; Maurino, V. Influence of Agglomeration and Aggregation on the Photocatalyticactivity of TiO$_2$ Nanoparticles. *Appl. Catal. B.* 2017, *216*, 80–87. DOI: 10.1016/j.apcatb.2017.05.046.

[55] Tolosana-Moranchel, A.; Pecharromán, C.; Faraldos, M.; Bahamonde, A. Strong Effect of Light Scattering by Distribution of TiO$_2$ Particle Aggregates on Photocatalytic Efficiency in Aqueous Suspensions. *Chem. Eng. J.* 2021, *403*, 126186. DOI: 10.1016/j.cej.2020.126186.

[56] Ozisik, M.N. ; In *Radiative Transfer and Interactions with Conduction and Convection* (New York: Wiley) 1–575 1973.

[57] Duderstadt, J.J., and Martin, R. *Transport Theory*; Whiley: New York, 1979.

[58] Brucato, A.; Rizzuti, L. Simplified Modeling of Radiant Fields in Heterogeneous Photoreactors. 1. Case of Zero Reflectance. *Ind. Eng. Chem. Res.* 1997, *36*(11), 4740–4747. DOI: 10.1021/ie960259j.

[59] Brucato, A.; Rizzuti, L. Simplified Modeling of Radiant Fields in Heterogeneous Photoreactors. 2. Limiting "Two-Flux" Model for the Case of Reflectance Greater than Zero. *Ind. Eng. Chem. Res.* 1997, *36*(11), 4748–4755. DOI: 10.1021/ie960260i.

[60] Loddo, V.; Addamo, M.; Augugliaro, V.; Palmisano, L.; Schiavello, M.; Garrone, E. Optical Properties and Quantum Yield Determination in Photocatalytic Suspensions. *AIChE J.* 2006, *52*(7), 2565–2574. DOI: 10.1002/aic.10883.

[61] Brucato, A.; Cassano, A. E.; Grisafi, F.; Montante, G.; Rizzuti, L.; Vella, G. Estimating Radiant Fields in Flat Heterogeneous Photoreactors by the Six-flux Model. *AIChE J.* 2006, *52*(11), 3882–3890. DOI: 10.1002/aic.10984.

[62] Grcic, I., and Puma, G.L. Six-flux absorption-scattering Models for Photocatalysis underwide-spectrum Irradiation Sources in Annular and Flat Reactors Usingcatalysts with Different Optical Properties. *Appl. Catal. B.* 2017, *211*, 222–234. DOI: 10.1016/j.apcatb.2017.04.014.

[63] Acosta-Herazo, R.; Monterriza-Romero, J.; Mueses, M.A.; Machuca-Martínez, F., and Puma, G.L. Coupling the Six Flux Absorption–Scattering Model to the Henyey–Greenstein Scattering Phase Function: Evaluation and Optimization of Radiation Absorption in Solar Heterogeneous Photoreactors. *Chem. Eng. J.* 2016, *302*, 86–96. DOI: 10.1016/j.cej.2016.04.127.

[64] Brusciglio, A.; Alfano, O. M.; Scargiali, F.; Brucato, A. A Probabilistic Approach to Radiant Field Modeling in Dense Particulate Systems. *Chem. Eng. Sci.* 2016, *142*, 79–88. DOI: 10.1016/j.ces.2015.11.025.

[65] Turolla, A.; Santoro, D.; de Bruyn, J.R.; Crapulli, F., and Antonelli, M. Nanoparticle Scattering Characterization and Mechanistic Modeling of UV-TiO$_2$ Photocatalytic Reactors Using Computational Fluid Dynamics. *Water Res.* 2016, *88*, 117–126. DOI: 10.1016/j.watres.2015.09.039.

[66] Ramírez-Cabrera, M.A.; Valadés-Velayo, P.J.; Arancibia-Bulnes, C.A., and Ramos, E. Validity of the Six-Flux Model for Photoreactors. *Chem. Eng. J.* 2017, *330*, 272–280. DOI: 10.1016/j.cej.2017.07.120.

[67] Romero, R.L.; Alfano, O.M., and Cassano, A.E. Cylindrical Photocatalytic Reactors. Radiation Absorption and Scattering Effects Produced by Suspended Fine Particles in an Annular Space. *Ind. Eng. Chem. Res.* 1997, *36*(8), 3094–3098. DOI: 10.1021/ie960664a.

[68] Sgalari, G.; Camera-Roda, G.; Santarelli, F. Int. Commun. Discrete Ordinate Method in the Analysis of Radiative Transfer in Photocatalytically Reacting Media. *Heat Mass Transfer*. 1998, *25*(5), 651–660. DOI: 10.1016/S0735-1933(98)00052-9.

[69] Camera-Roda, G.; Santarelli, F. A Rational Approach to the Design of Photocatalytic Reactors. *Ind. Eng. Chem. Res.* 2007, *46*, 7637–7644. DOI: 10.1021/ie070302a.

[70] Pareek, V.; Chong, S.; Tadé, M., and Adesina, A.A. Light Intensity Distribution in Heterogenous Photocatalytic Reactors. *Asia Pac. J. Chem. Eng.* 2008, *3*(2), 171–201. DOI: 10.1002/apj.129.

[71] Spadoni, G.; Bandino, E.; Santarelli, F. Scattering Effects in Photosensitized Reactions. *Chem. Eng. Sci.* 1978, *33*(4), 517–524. DOI: 10.1016/0009-2509(78)80012-8.

[72] Pasquali, M.; Santarelli, F.; Porter, J.F., and Yue, P.L. Radiative Transfer in Photocatalytic Systems. *AIChE J.* 1996, *42*(2), 532–537. DOI: 10.1002/aic.690420222.

[73] Pareek, V.K.; Cox, S.J.; Brungs, M.P.; Young, B., and Adesina, A.A. Computational Fluid Dynamic (CFD) Simulation of a pilot-scale Annular Bubble Column Photocatalytic Reactor. *Chem. Eng. Sci.* 2003, *58*(3–6), 859–865. DOI: 10.1016/S0009-2509(02)00617-6.

[74] Marugán, J.; van Grieken, R.; Pablos, C.; Satuf, M.L.; Cassano, A.E., and Alfano, O.M. Modeling of a bench-scale Photocatalytic Reactor for Water Disinfection from laboratory-scale Kinetic Data. *Chem. Eng. J.* 2013, *224*, 39–45. DOI: 10.1016/j. cej.2012.11.082.

[75] Fontelles-Carceller, O.; Muñoz-Batista, M.J.; Rodríguez-Castellón, E.; Conesa, J.C.; Fernández-García, M., and Kubacka, A. Measuring and Interpreting Quantum Efficiency for Hydrogen Photoproduction Using Pt-titania Catalysts. *J. Catal.* 2017, *347*, 157–169. DOI: 10.1016/j.jcat.2017.01.012.

[76] Duran, J.E.; Taghipour, F., and Mosheni, M. Irradiance Modeling in Annular Photoreactors Using the finite-volume Method. *J. Photochem. Photobiol. A.* 2010, *215* (1), 81–89. DOI: 10.1016/j.jphotochem.2010.07.027.

[77] Huang, Q.; Liu, T.; Yang, J.; Yao, L.; Gao, L. Evaluation of Radiative Transfer Using the Finite Volume Method in Cylindrical Photoreactors. *Chem. Eng. Sci.* 2011, *66*(17), 3930–3940. DOI: 10.1016/j.ces.2011.05.032.

[78] Yang, Q.; Ang, P.L.; Ray, M.B., and Pehkonen, S.O. Light Distribution Field in Catalyst Suspensions within an Annular Photoreactor. *Chem. Eng. Sci.* 2005, *60*(19), 5255–5268. DOI: 10.1016/j.ces.2005.02.067.

[79] Zekri, M.; Juntin-Colbeau, C. A Mathematical Model to Describe the Photocatalytic Reality: What Is the Probability that A Photon Does Its Job? *Chem. Eng. J.* 2013, *225*, 547–557. DOI: 10.1016/j.cej.2013.03.129.

[80] Moreira, J.; Serrano, B.; Ortíz, A.; de Lasa, H. Evaluation of Photon Absorption in an Aqueous TiO_2 Slurry Reactor Using Monte Carlo Simulations and Macroscopic Balance. *Ind. Eng. Chem. Res.* 2010, *49*(21), 10524–10529. DOI: 10.1021/ie100374f.

[81] Valadés-Pelayo, P.J.; Moreira Del Rio, J.; Solano-Flores, P.; Serrano, B., and de Lasa, H. Establishing Photon Absorption Fields in a Photo-CREC Water II Reactor Using a CREC-spectroradiometric Probe. *Chem. Eng. Sci.* 2014, *116*, 406–417. DOI: 10.1016/j. ces.2014.04.041.

[82] Tong, K.; Yang, L.; Du, X. Modelling of TiO_2-based Packing Bed Photocatalytic Reactor with Raschig Rings for Phenol Degradation by Coupled CFD and DEM. *Chem. Eng. J.* 2020, *400*, 125988. DOI: 10.1016/j.cej.2020.125988.

[83] Zhang, L., and Anderson, W.A. A Finite Model for the Prediction of the UV Radiation Field around A Linear Lamp. *Chem. Eng. Sci.* 2010, *65*(5), 1513–1521. DOI: 10.1016/j. ces.2009.10.013.

[84] Esteban Durán, J.; Taghipour, F.; Mohseni, M. Irradiance Modeling in Annular Photoreactors Using the finite-volume Method. *J. Photochem. Photobiol. A.* 2010, *215* (1), 81–89. DOI: 10.1016/j.jphotochem.2010.07.027.

[85] Boyjoo, Y.; Ang, M.; Pareek, V. Lamp Emission and Quartz Sleeve Modeling in Slurry Photocatalytic Reactors. *Chem. Eng. Sci.* 2014, *111*, 34–40. DOI: 10.1016/j. ces.2014.02.023.

[86] Moreno, J.; Casada, C.; Marugán, J. Improved Discrete Ordinate Method for Accurate Simulation Radiation Transport Using Solar and LED Light Sources. *Chem. Eng. J.* 2019, *205*, 151–164. DOI: 10.1016/j.ces.2019.04.034.

[87] Lugo-Vega, C.S.; Serrano-Rosales, B., and de Lasa, H. Immobilized Particle Coating for Optimum Photon and TiO_2 Utilization in Scaled Air Treatment Photo Reactors. *Appl. Catal. B.* 2016, *198*, 211–223. DOI: 10.1016/j.apcatb.2016.05.063.

[88] Bolton, J.R. Calculation of Ultraviolet Fluence Rate Distributions in an Annular Reactor: Significance of Refraction and Reflection. *Water Res.* 2000, *34*(13), 3315–3324. DOI: 10.1016/S0043-1354(00)00087-7.

[89] Muñoz-Batista, M.J.; Kubacka, A.; Hungría, A.B., and Fernández-García, M. Heterogeneous Photocatalysis: Light-matter Interaction and Chemical effects in Quantum Efficiency Calculations. *J. Catal.* 2015, *330*, 154–166. DOI: 10.1016/j.jcat.2015.06.021.

[90] Alexadis, A.; Baldi, G.; Mazzarino, I. Modeling of a Photocatalytic Reactor with A fixed Bed Supported Catalyst. *Catal. Today.* 2001, *66*(2–4), 467–474. DOI: 10.1016/S0920-5861(01)00255-3.

[91] Vaiano, V.; Sacco, O.; Pisano, D.; Sannino, D.; Ciambelli, P. From the Design to the Development of a Continuous Fixed Bed Photoreactor for Photocatalytic Degradation of Organic Pollutants in Wastewater. *Chem. Eng. Sci.* 2015, *137*, 152–160. DOI: 10.1016/j.ces.2015.06.023.0009-2509.

[92] Eduards, D.K. Solar Absorption by Each Element in an absorber-coverglass Array. *Sol. Ener.* 1977, *19*, 401–402. DOI: 10.1016/0038-092X(77)90013-5.

[93] Salvadores, F.; Minen, R.J.; Carballada, J.; Alfano, O.M., and Ballari, M.M. Kinetic Study of Acetaldehyde Degradation in Gas Phase Applying Visible Light Photocatalysis. *Chem. Eng. Technol.* 2016, *39*(1), 166–174. DOI: 10.1002/ceat.201500507.

[94] Changrani, R.G., and Raupp, G.B. Monte Carlo Simulation of the Radiation Field in a Reticulated Foam Photocatalytic Reactor. *AIChE J.* 1999, *45*(5), 829–842. DOI: 10.1002/aic.690450516.

[95] Loddo, V.; Yurdakal, S.; Palmisano, G.; Imoberdorf, G.E.; Irazoqui, H.A.; Alfano, O.M.; Augugliaro, V.; Berber, H., and Palmisano, L. Selective Photocatalytic Oxidation of 4-methoxybenzyl Alcohol Tp p-anisaldehyde in organic-free Water in a Continuous Annular Fixed Bed Reactor. *Int. J. Chem. Reactor Eng.* 2007, *5*(1), A57. DOI: 10.2202/1542-6580.1500.

[96] Zazueta, A.L.L.; Destaillats, H., and Li Puma, G. Radiation Field Modeling and Optimization of a Compact and Modular multi-plate Photocatalytic Reactor (MPPR) for air/water Purification by Monte Carlo Method. *Chem. Eng. J.* 2013, *217*, 475–485. DOI: 10.1016/j.cej.2012.11.085.

[97] Padoin, N.; Soares, C. An Explicit Correlation for Optimal TiO_2 Film Thickness in Immobilized Photocatalytic Reaction Systems. *Chem. Eng. J.* 2017, *310*, 381–388. DOI: 10.1016/j.cej.2016.06.013.

[98] Emeline, A.V.; Frolov, A.V.; Ryabchuk, V.K., and Serpone, N. Spectral Dependencies of the Quantum Yield of Photochemical Processes on the Surface of Nano/Micro-Particulates of Wide-Band-Gap Metal Oxides. IV. Theoretical Modeling of the Activity and Selectivity of Semiconductor Photocatalysts with Inclusion of a Sub. *J. Phys. Chem. B.* 2003, *107*, 7109–7119. DOI: 10.1021/jp030126t.

[99] Caudillo-Flores, U.; Muñoz-Batista, M.J.; Hungría, A.B.; López Haro, M.; Fernández-García, M., and Kubacka, A. Toluene and Styrene photo-oxidation Quantum Efficiency: Comparison between Doped and Composite tungsten-containing anatase-based Catalysts. *Appl. Catal. B.* 2019, *245*, 49–61. DOI: 10.1016/j.apcatb.2018.12.032.

[100] Fontelles-Carceller, O.; Muñoz-Batista, M.J.; Fernández-García, M., and Kubacka, A. Interface Effects in Sunlight-Driven Ag/g-C 3 N 4 Composite Catalysts: Study of the Toluene Photodegradation Quantum Efficiency. *ACS Appl. Mater. Interfaces.* 2016, *8*(4), 2617–2627. DOI: 10.1021/acsami.5b10434.

[101] Fontelles-Carceller, O.; Muñoz-Batista, M.J.; Conesa, J.C.; Kubacka, A., and Fernández-García, M. H 2 photo-production from Methanol, Ethanol and 2-propanol:Pt-(Nb)TiO 2 Performance under UV and Visible Light. *Mol. Catal.* 2018, *446*, 88–97. DOI: 10.1016/j.mcat.2017.12.023.

[102] Caudillo-Flores, U.; Muñoz-Batista, M.J.; Fernández-García, M., and Kubacka, A. Bimetallic Pt-Pd co-catalyst Nb-doped TiO_2 Materials for H_2 photo-production under UV and Visible Light Illumination. *Appl. Catal. B.* 2018, *238*, 533–545. DOI: 10.1016/j.apcatb.2018.07.047.

[103] Narayanan, N.; Nair, M. V. H.; Viswanathan, B. On the Current Status of the Mechanism Aspects of Photocatalytic Reduction of Carbon Doixide. *Indian J. Chem.* 2017, *36A*, 251–269. http://nopr.niscair.res.ind/123456789/40911.

[104] Caudillo-Flores, U.; Avilés-García, O.; Alonso-Núñez, G.; Kubacka, K.; Fernández-García, M. Assessing Quantitatively Charge Carrier Fate in 4-Chlorophenol Photocatalytic Degradation Using Globular Titania Catalysts: Implications in Quantum Efficiency Calculation. *J. Environ. Chem. Eng.* 2021, *9*, 106074. DOI:10.1016/j.jece.2021.106074. 5

[105] Ismael, M. Latest Progress on the Key Operating Parameters Affecting the Photocatalytic Activity of TiO_2-based Photocatalysts for Hydrogen Fuel Production: A Comprehensive Review. *Fuel.* 2021, *303*, 121207. DOI: 10.1016/j.fuel.2021.121207.

[106] Imoberdorf, G.E.; Cassano, A.E.; Irazoqui, H.A., and Alfano, O.M. Simulation of a multi-annular Photocatalytic Reactor for Degradation of Perchloroethylene in Air: Parametric Analysis of Radiative Energy Efficiencies. *Chem. Eng. Sci.* 2007, *64*(4), 1138–1154. DOI: 10.1016/j.ces.2006.10.024.

[107] Passalía, C.; Alfano, O.M., and Brandi, R.J. Optimal Design of a corrugated-wall Photocatalytic Reactor Using Efficiencies in Series and Computational Fluid Dynamics (CFD) Modeling. *Ind. Eng. Chem. Res.* 2013, *52*(21), 6916–6922. DOI: 10.1021/ie302838m.

[108] Muñoz-Batista, M.J.; Ballari, M.M.; Kubacka, A.; Cassano, A.E.; Alfano, O.M., and Fernández-García, M. Acetaldehyde Degradation under UV and Visible Irradiation Using CeO_2–TiO_2 Composite Systems: Evaluation of the Photocatalytic Efficiencies. *Chem. Eng. J.* 2014, *255*, 297–306. DOI: 10.1016/j.cej.2014.06.056.

[109] Martín-Sómer, M.; Pablos, C.; van Grieken, R.; Marugán, J. Influence of Light Distribution on the Performance of Photocatalytic Reactors: LED Vs Mercury Lamps. *Appl. Catal. B.* 2017, *215*, 1–7. DOI: 10.1016/j.apcatb.2017.05.048.

[110] Tokode, O.; Prabhu, R.; Lawton, L.A., and Robertson, P.K.J. UV LED Sources for Heterogeneous Photocatalysis, in. In *Environ. Photochem. Part III*, Springer Verlag: 2014; Vol. , pp 159–179.

[111] Khodadadian, F.; De Boer, M.W.; Poursaeidesfahani, A.; Van Ommen, J.R.; Stankiewicz, A.I., and Lakerveld, R. Design, Characterization and Model Validation of a LED-based Photocatalytic Reactor for Gas Phase Applications. *Chem. Eng. J.* 2018, *333*, 456–466. DOI: 10.1016/j.cej.2017.09.108.

[112] Bandala, E.R.; Arancibia-Bulnes, C.A.; Orozco, S.L., and Estrada, C.A. Solar Photoreactors Comparison Based on Oxalic Acid Photocatalytic Degradation. *Sol. Energy.* 2004, *77*(5), 503–512. DOI: 10.1016/j.solener.2004.03.021.

[113] Imoberdorf, G.E.; Cassano, A.E.; Irazoqui, H.A., and Alfano, O.M. Optimal Design and Modeling of Annular Photocatalytic Wall Reactors. *Catal. Today.* 2007, *129*(1–2), 118–126. DOI: 10.1016/j.cattod.2007.06.057.

[114] De Lasa, H.I.; Serrano, B., and Salaices, M. *Photocatalytic Reaction Engineering.*New York, USA: Springer Science+Business Media, LLC;2005.

[115] Hisatomi, T.; Domen, K. Reaction Systems for Solar Hydrogen Production via Water Splitting with Particulate Semiconductor Photocatalysts. *Nat. Catal.* 2020, *2*(5), 387–399. DOI: 10.1038/s41929-019-0242-6.

[116] Muñoz-Batista, M.J.; Eslava-Castillo, A.M.; Kubacka, A., and Fernández-García, M. Thermo-photo Degradation of 2-propanol Using a Composite ceria-titania Catalyst: Physico-chemical Interpretation from a Kinetic Model. *Appl. Catal. B.* 2018, *225*, 298–306. DOI: 10.1016/j.apcatb.2017.11.073.

[117] Zhang, J.; Nosaka, Y. Quantitative Detection of OH Radicals for Investigating the Reaction Mechanism of Various Visible-Light TiO$_2$ Photocatalysts in Aqueous Suspension. *J. Phys. Chem. C.* 2013, *117*(3), 1383–1391. DOI: 10.1021/jp3105166.

[118] Muñoz-Batista, M.J.; Ballari, M.M.; Cassano, A.E.; Alfano, O.M.; Kubacka, A., and Fernández-García, M. Ceria Promotion of Acetaldehyde photo-oxidation in a TiO$_2$-based Catalyst: A Spectroscopic and Kinetic Study. *Catal. Sci. Technol.* 2014, *5*(3), 1521–1531. DOI: 10.1039/C4CY01293C.

[119] Muñoz-Batista, M.J.; Gómez-Cerezo, M.N.; Kubacka, A.; Tudela, D., and Fernández-García, M. Role of Interface Contact in CeO$_2$–tio$_2$ Photocatalytic Composite Materials. *ACS Catal.* 2014, *4*(1), 63–72. DOI: 10.1021/cs400878b.

[120] Muñoz-Batista, M.J.; Kubacka, A., and Fernández-García, M. Effective Enhancement of TiO$_2$ Photocatalysis by Synergistic Interaction of Surface Species: From Promoters to Co-catalysts. *ACS Catal.* 2014, *4*(12), 4277–4288. DOI: 10.1021/cs501408u.

[121] Gu, Q.; Long, J.; Fan, L.; Chen, L.; Zhao, L.; Lin, H.; Wan, X. Single-site Sn-grafted Ru/TiO$_2$ Photocatalysts for Biomass Reforming: Synergistic Effect of Dual co-catalysts and Molecular Mechanism. *J. Catal.* 2013, *303*, 141–155. DOI: 10.1016/j.jcat.2013.03.014.

[122] Muñoz-Batista, M.J.; Kubacka, A.; Gómez-Cerezo, M.N.; Tudela, D., and Fernández-García, M. Sunlight-driven Toluene photo-elimination Using CeO$_2$-TiO$_2$ Composite Systems: A Kinetic Study. *Appl. Catal. B.* 2013, *140–141*, 626–635. DOI: 10.1016/j.apcatb.2013.04.071.

[123] Cunningham, J.; Srijaranai, S. Isotope-effect Evidence for Hydroxyl Radical Involvement in Alcohol photo-oxidation Sensitized by TiO$_2$ in Aqueous Suspension. *J. Photochem. Photobiol. A.* 1988, *43*(3), 329–335. DOI: 10.1016/1010-6030(88)80029-7.

[124] Lin, X.H.; Miao, Y., and Li, S.F.Y. Location of Photocatalytic Oxidation Processes on Anatase Titanium Dioxide. *Catal. Sci. Technol.* 2017, *7*(2), 441–451. DOI: 10.1039/C6CY02214F.

[125] Chiarello, G.L.; Ferri, D., and Selli, E. Effect of the CH$_3$OH/H$_2$O Ratio on the Mechanism of the gas-phase Photocatalytic Reforming of Methanol on Noble metal-modified TiO$_2$. *J. Catal.* 2011, *289*(2), 168–177. DOI: 10.1016/j.jcat.2011.03.013.

[126] Yin, G.; Huang, X.; Chen, T.; Zhao, W.; Bi, Q.; Xu, J.; Han, Y.; Huang, F. Hydrogenated Blue Titania for Efficient Solar to Chemical Conversions: Preparation, Characterization, and Reaction Mechanism of CO$_2$ Reduction. *ACS Catal.* 2018, *8*(2), 1009–1017. DOI: 10.1021/acscatal.7b03473.

[127] Arsac, F.; Bianchi, D.; Chovelon, J. M.; Ferronato, C.; Herrman, J. M. Experimental Microkinetic Approach of the Photocatalytic Oxidation of Isopropyl Alcohol on TiO$_2$. Part 2. From the Surface Elementary Steps to the Rates of Oxidation of the C$_3$H$_X$O Species. *J. Phys. Chem. A.* 2006, *110*(12), 4213–4222. DOI: 10.1021/jp057255p.

[128] Topalian, Z.; Stefanov, B.I.; Granqvist, C.G., and Osterlund, L. Adsorption and photo-oxidation of Acetaldehyde on TiO$_2$ and sulfate-modified TiO$_2$: Studies by in Situ FTIR Spectroscopy and micro-kinetic Modeling. *J. Catal.* 2013, *307*, 265–274. DOI: 10.1016/j.jcat.2013.08.004.

[129] Mattsson, A.; Leideborg, M.; Larsson, K.; Westing, G.; Osterlund, L. Adsorption and Solar Light Decomposition of Acetone on Anatase TiO$_2$ and Niobium Doped TiO$_2$ Thin Films. *J. Phys. Chem. B.* 2006, *110*(3), 1210–1220. DOI: 10.1021/jp055656z.

[130] Walenta, C.A.; Courtois, C.; Kollmannsberger, S.L.; Eder, M.; Tschurl, M., and Heiz, U. Surface Species in Photocatalytic Methanol Reforming on Pt/TiO$_2$ (110): Learning from Surface Science Experiments for Catalytically Relevant Conditions. *ACS Catal.* 2020, *10* (7), 4080–4091. DOI: 10.1021/acscatal.0c00260.

[131] Ollis, D.F. Kinetics of Liquid Phase Photocatalyzed Reactions: An Illuminating Approach. *J. Phys. Chem. B.* 2005, *109*(6), 2439–2444. DOI: 10.1021/jp040236f.

[132] Nosaka, Y., and Nosaka, A.Y. Langmuir-Hinshelwood and Light-Intensity Dependence Analyses of Photocatalytic Oxidation Rates by Two-Dimensional-Ladder Kinetic Simulation. *J. Phys. Chem. C.* 2018, *122*(50), 28748–28756. DOI: 10.1021/acs.jpcc.8b09421.

[133] Herrmann, J.M. Heterogeneous Photocatalysis: Fundamentals and Applications to the Removal of Various Types of Aqueous Pollutants. *Catal. Today.* 1999, *53*(1), 115–129. DOI: 10.1016/S0920-5861(99)00107-8.

[134] Migani, A.; Blancafort, L. Excitonic Interfacial Proton-Coupled Electron Transfer Mechanism in the Photocatalytic Oxidation of Methanol to Formaldehyde on TiO$_2$ (110). *J. Am. Chem. Soc.* 2016, *138*(49), 16165–16173. DOI: 10.1021/jacs.6b11067.

[135] Migani, A.; Blancafort, L. What Controls Photocatalytic Water Oxidation on Rutile TiO$_2$ (110) under Ultra-High-Vacuum Conditions? *J. Am. Chem. Soc.* 2017, *139*(34), 11845–11856. DOI: 10.1021/jacs.7b05121.

[136] Satuf, M.L.; Bradi, R.J.; Cassano, A.E., and Alfano, O.M. Photocatalytic Degradation of 4-chlorophenol: A Kinetic Study. *Appl. Catal. B.* 2008, *82*(1–2), 37–49. DOI: 10.1016/j.apcatb.2008.01.003.

[137] Marugán, J.; van Grieken, R.; Cassano, A.E., and Alfano, O.M. Intrinsic Kinetic Modeling with Explicit Radiation Absorption Effects of the Photocatalytic Oxidation of Cyanide with TiO$_2$ and silica-supported TiO$_2$ Suspensions. *Appl. Catal. B.* 2008, *85*(1–2), 48–60. DOI: 10.1016/j.apcatb.2008.06.026.

[138] Mueses, M.A.; Machuca-Martínez, F., and Puma, G.L. Effective Quantum Yield and Reaction Rate Model for Evaluation of Photocatalytic Degradation of Water Contaminants in Heterogeneous pilot-scale Solar Photoreactors. *Chem. Eng. J.* 2013, 215–216, 937–947. DOI: 10.1016/j.cej.2012.11.076.

[139] Salvadores, F.; Minen, R.I.; Carballada, J.; Alfano, O.M., and Ballari, M.M. Kinetic Study of Acetaldehyde Degradation Applying Visible Light Photocatalysis. *Chem. Eng. Technol.* 2016, *39*(1), 166–174. DOI: 10.1002/ceat.201500507.

[140] Zalazar, C.S.; Romero, R.L.; Martín, C.A., and Cassano, A.E. Photocatalytic Intrinsic Reaction Kinetics I: Mineralization of Dichloroacetic Acid. *Chem. Eng. Sci.* 2005, *60*(19), 5240–5254. DOI: 10.1016/j.ces.2005.04.050.

[141] Ballari, M.M.; Cassano, A.E., and Alfano, O.M. Photocatalytic Degradation of Dichloroacetic Acid. A Kinetic Study with A Mechanistically Based Reaction Model. *Ind. Eng. Chem. Res.* 2009, *48*(4), 1847–1858. DOI: 10.1021/ie801194f.

[142] Barba-Nieto, I.; Caudillo-Flores, U.; Gómez-Cerezo, M.N.; Kubacka, A., and Fernández-García, M. Boosting Pt/TiO$_2$ Hydrogen Photoproduction through Zr Doping of the Anatase Structure: A Spectroscopic and Mechanistic Study. *Chem. Eng. J.* 2020, *398*, 125665. DOI: 10.1016/j.cej.2020.125665.

[143] Monllor-Satoca, D.; Gómez, R.; González-Hidalgo, M.; Salvador, P. The "Direct–Indirect" Model: An Alternative Kinetic Approach in Heterogeneous Photocatalysis Based on the Degree of Interaction of Dissolved Pollutant Species with the Semiconductor Surface. *Catal. Today.* 2007, *129*(1–2), 247–255. DOI: 10.1016/j.cattod.2007.08.002.

[144] Montolla, J.F.; Peral, J., and Salvador, P. The direct–indirect Kinetic Model in Photocatalysis: A Reanalysis of Phenol and Formic Acid Degradation Rate Dependence on Photon Flow and Concentration in TiO$_2$ Aqueous Dispersions. *Appl. Catal. B*. 2009, *88*(1–2), 50–59. DOI: 10.1016/j.apcatb.2008.09.035.

[145] Montolla, J.F.; Peral, J., and Salvador, P. Comprehensive Kinetic and Mechanistic Analysis of TiO$_2$ Photocatalytic Reactions according to the Direct–Indirect Model: (I) Theoretical Approach. *J. Phys. Chem. C*. 2014, *118*(26), 14266–14275. DOI: 10.1021/jp4121645.

[146] Turchi, C., and Ollis, D.F. Photocatalytic Degradation of Organic Water Contaminants: Mechanisms Involving Hydroxyl Radical Attack. *J. Catal.* 1990, *122*(1), 178–192. DOI: 10.1016/0021-9517(90)90269-P.

[147] Acosta-Herazo, R.; Cañaveral-Velásquez, B.; Pérez-Giraldo, K.; Mueses, M.A.; Pinzón-Cárdenas, M.H., and Machuca-Martínez, F. A MATLAB-Based Application for Modeling and Simulation of Solar Slurry Photocatalytic Reactors for Environmental Applications. *Water*. 2020, *12*(8), 2196–2212. DOI: 10.3390/w12082196.

[148] Mul, G.; Wasylenko, W.; Handy, M.S., and Frey, H. Cyclohexene photo-oxidation over Vanadia Catalyst Analyzed by Time Resolved ATR-FT-IR Spectroscopy. *Phys. Chem. Chem. Phys.* 2008, *10*(21), 3131–3137. DOI: 10.1039/B800314A.

[149] Elser, M. J.; Diwald, O. Facilitated Lattice Oxygen Depletion in Consolidated TiO$_2$ Nanocrystal Ensembles: A Quantitative Spectroscopic O$_2$ Adsorption Study.*J. Phys. Chem. C* 2012, *116*, 2896–2903.DOI:10.1021/jp208707p

[150] Sobanska, K.; Krasowka, A.; Mazur, T.; Podolska-Serafin, K.; Pietrzyk, P., and Sojka, Z. Diagnostic Features of EPR Spectra of Superoxide Intermediates on Catalytic Surfaces and Molecular Interpretation of Their *g* and *A* Tensors. *Top. Catal.* 2015, *58*(12–13), 796–810. DOI: 10.1007/s11244-015-0420-y.

[151] Malayeri, M.; Haghighat, F.; Lee, C.-S. Kinetic Modeling of the photocatalytic degradation of methyl ethyl ketone in air for a continuous-flow reactor. *Chem. Eng. J.* 2021, *404*, 126602. DOI: 10.1016/j.cej.2020.126602.

[152] Caudillo-Flores, U.; Muñoz-Batista, M.J.; Luque, R.; Fernández-García, M., and Kubacka, A. g-C$_3$N$_4$/TiO$_2$ composite catalysts for the photo-oxidation of toluene: Chemical and charge handling effects. *Chem. Eng. J.* 2019, *378*, 122228. DOI: 10.1016/j.cej.2019.122228.

[153] Caudillo-Flores, U.; Fernández-García, M.; Kubacka, A. Photocatalytic toluene degradation: Braiding physico-chemical and Intrinsic Kinetic Analyses. *React. Chem. Eng.* 2020, *5*(8), 1429–1440. DOI: 10.1039/d0re00211a.